$Na_V1.1$ in mammalian sensory neurons is required for normal motor behaviors

Cyrrus M. Espino[1†], Cheyanne M. Lewis[1†], Serena Ortiz[2], Miloni S. Dalal[3], Kaylee M. Wells[4], Darik A. O'Neil[4], Katherine A. Wilkinson[2], and Theanne N. Griffith[1,4*]

[1]*Department of Physiology and Membrane Biology, University of California Davis, Davis, CA, 95616*
[2]*Department of Biological Science, San José State University, San José, CA, 95192*
[3]*Department of Pharmacology, Physiology, and Neuroscience, New Jersey Medical School-Rutgers University, Newark, NJ, 07103*
[4]*Neurobiology course, Marine Biological Laboratory Woods Hole, MA, 02540*

*Corresponding Author: Theanne N. Griffith
1275 Med Science Drive
Tupper Hall 4135
Davis, CA 95616
530.754.2780
tgriffith@ucdavis.edu

†These authors contributed equally to this work.
Conflicts of Interest: None to declare

Acknowledgements: This research was supported by a Postdoctoral Enrichment Program Award from the Burroughs Welcome Fund (TNG) and by 5T32GM099608-10 (CME). Work at San José State was supported by NIGMS 5SC3GM127195 (KAW) and NIGMS 5R25GM71381 (SO). Core facilities were supported by P30 EY12576. Part of this project was carried out at the Marine Biological Laboratory Neurobiology Course, with support from NINDS R25NS063307. Thanks to Drs. Jon Sack and Xinzhong Dong for sharing mouse lines, Drs. Jorge Contreras and Ioana Carcea for sharing behavioral equipment, Miguel Gonzalez Fernandez for writing code to automate *ex vivo* data analysis, and members of the Griffith laboratory for helpful discussions.

ABSTRACT

The mammalian voltage-gated sodium channel (Na_V), $Na_V1.1$, has been well-studied in the central nervous system; conversely, its contribution to peripheral sensory neuron function is more enigmatic. Here, we report a new role for peripherally expressed $Na_V1.1$ in murine motor behaviors. RNAscope analysis found 100% of proprioceptors express $Na_V1.1$ transcript, consistent with *in vitro* patch clamp recordings showing this channel is required for repetitive firing in proprioceptors. Notably, genetic deletion of $Na_V1.1$ in all sensory neurons caused profound motor coordination deficits in homozygous conditional knockout animals of both sexes, a phenotype similar to conditional Piezo2-knockout animals. Movement deficits were also observed in heterozygotes, demonstrating that $Na_V1.1$ haploinsufficiency in sensory neurons leads to motor deficiencies. This behavioral phenotype was not due to reduced proprioceptor numbers or abnormal muscle spindle formation; however, we observed decreased proprioceptor innervation of motor neurons in the spinal cord in conditional knockouts, indicating loss of $Na_V1.1$ in sensory neurons alters spinal cord circuitry. *Ex vivo* muscle afferent recordings also support the notion that loss of $Na_V1.1$ leads to aberrant proprioceptor function. Collectively, these data provide the first evidence that $Na_V1.1$ in mammalian sensory neurons is essential for motor coordination. Importantly, human patients harboring $Na_V1.1$ loss-of-function mutations often present with motor delays and ataxia. Thus, our data suggest sensory neuron dysfunction may contribute to the clinical manifestations and co-morbidities of neurological disorders in which $Na_V1.1$ function is compromised.

INTRODUCTION

Voltage gated sodium channels (Na_Vs) are critical mediators of neuronal excitability and are responsible for action potential generation and propagation (Ahern et al., 2016; Bean, 2007) . In the mammalian nervous system there are nine isoforms (Na_V1.1-1.9), each with unique biophysical properties, as well as distinguishing cellular expression and subcellular localization patterns (Bennett et al., 2019; Catterall, 2017). Of these different subtypes, Na_V1.1 is notable for its role in brain disease (Escayg and Goldin, 2010; Mulley et al., 2005; Ogiwara et al., 2007). Indeed, *Scn1a*, the gene that encodes Na_V1.1, is referred to as a "super culprit" gene, with over 1,000 associated mutations that lead to abnormal brain function, resulting in brain disorders such as epilepsy and migraine, as well as neurodivergent phenotypes, such as autism spectrum disorder (Ding et al., 2021; Lossin, 2009). Homozygous $Na_V1.1^{-/-}$ global knockout mice are ataxic and die by P15, while heterozygous $Na_V1.1^{+/-}$ animals develop seizures and begin to die sporadically starting at P21 (Yu et al., 2006). In addition to the central nervous system, Na_V1.1 is also expressed in the peripheral nervous system (Sharma et al., 2020; Usoskin et al., 2015); yet, the prominent role this channel plays in brain function has left its physiological roles in sensory neuron populations understudied.

Peripheral sensory neurons of the dorsal root and trigeminal ganglia (DRG and TG, respectively) are tasked with encoding somatic sensations, such as touch, temperature, pain, and proprioception, and are anatomically and functionally heterogenous (Kupari et al., 2021; Nguyen et al., 2021; Oliver et al., 2021; Wu et al., 2021). Na_V1.1 transcript and protein have been observed primarily in myelinated mechanosensory DRG and TG neurons (Fukuoka et al., 2008; Ho and O'Leary, 2011; Osteen et al., 2016). Indeed, subcutaneous injection of the Na_V1.1 activator, Hma1, into mouse hind paw causes non-inflammatory mechanical pain and spontaneous pain behaviors (Osteen et al., 2016). Interestingly, pharmacological inhibition of Na_V1.1 does not affect mechanical thresholds in uninjured mice but does reduce mechanical pain in a spared-nerve

injury model (Salvatierra et al., 2018), suggesting $Na_V1.1$ may have a more prominent role in mechanical pain as opposed to normal touch sensing. $Na_V1.1$ in TG neurons has also been reported to mediate mechanical pain in an orbitofacial chronic constriction injury model (Pineda-Farias et al., 2021). In addition to somatosensory neurons, $Na_V1.1$ is found in colon-innervating vagal neurons, where it contributes to firing of colonic mechano-nociceptors and is upregulated in a mouse model of chronic visceral hypersensitivity (Osteen et al., 2016; Salvatierra et al., 2018). Lastly, $Na_V1.1$ contributes to action potential firing in a subset of DRG neurons that express the cold sensitive ion channel, transient receptor potential melastatin 8 (TRPM8), suggesting the channel may also contribute to thermosensory transmission (Griffith et al., 2019). While most data support a role for $Na_V1.1$ in pain, the limited number of studies that have investigated $Na_V1.1$ function in sensory neurons has left gaps in our knowledge regarding other potential roles this channel may play in somatosensation.

Given the relatively under-explored role of $Na_V1.1$ in the peripheral nervous system, we set out to determine what other somatosensory modalities rely on $Na_V1.1$ expression in sensory neurons. Here, we show that 100% of proprioceptors express $Na_V1.1$ mRNA. A functional role for the channel in these cells was supported by both *in vitro* and *ex-vivo* electrophysiological recordings from genetically identified proprioceptors and functionally identified muscle spindle afferents, respectively. Importantly, mice lacking $Na_V1.1$ in all sensory neurons display visible and profound motor deficits and ataxic-like behavior, which were quantified in rotarod and open field assays. These deficits may be due to a combination of aberrant electrical signaling and altered spinal cord circuitry. Collectively, our data provide evidence for a new role for peripherally expressed $Na_V1.1$ in proprioceptor function and motor coordination.

MATERIALS AND METHODS

Key resources. **Table 1** contains a list of key resources and supplies used for this study.

Reagent or Resource	Source	Identifier
Deposited Data		
Source data	This paper	doi: 10.17632/kt23th75v9.2
Matlab scripts	This paper	https://github.com/doctheagrif/Current-Clamp-Matlab-Code_O-Neil-DA
Antibodies		
Rabbit polyclonal anti-DsRed	Takara Bio	Catalogue #632496
Chicken polyclonal GFP	Abcam	Catalogue #ab13970
Chicken polyclonal NFH	Abcam	Catalogue #ab4680
Rabbit polyclonal CGRP	Immunostar	Catalogue #24112
Guinea pig polyclonal VGLUT1	Thomas Jessell Laboratory; HHMI Columbia University	Catalogue #CU1706, RRID:AB_2665455
Chicken polyclonal β3-tubulin	Abcam	Catalogue #ab41489
Rabbit polyclonal β3-tubulin	Abcam	Catalogue #ab18207
Chemicals		
VECTASHIELD® Antifade Mounting Media with DAPI	Vector Laboratories	Catalogue #H-2000
Tissue-Tek OCT compound	Sakura	Catalogue #4583
Fluromount-G DAPI	SouthernBiotech	Catalogue #0100-20
Laminin	Sigma-Aldrich	Catalogue #L2020-1MG
Collagenase type P	Sigma-Aldrich	Catalogue #11213865001
TrypLE Express	ThermoFisher	Catalogue #12605-010
MEM	ThermoFisher	Catalogue #11095-080
Penicillin-streptomycin	ThermoFisher	Catalogue #15140-122
MEM vitamin solution	ThermoFisher	Catalogue #11120-052
B-27 supplement	ThermoFisher	Catalogue #17504-044
Horse serum, heat inactivated	ThermoFisher	Catalogue #26050-070
ICA 121431	Tocris Bioscience	Catalogue #5066/10
Critical Commercial Assays		
RNAscope Fluorescence Multiplex Kit	Advanced Cell Diagnostics	Catalogue #320851
Oligonucleotides		
Pvalb probe channel 1	Advanced Cell Diagnostics	Catalogue #421931
Scn1a probe channel 2	Advanced Cell Diagnostics	Catalogue #556181-C2
Runx3 probe channel 3	Advanced Cell Diagnostics	Catalogue #451271-C3
Experimental Models: Mouse Strains		
$Pirt^{cre}$	Dr. Xinzhong Dong	
$Rosa26^{Ai14}$	Jackson Laboratories	Stock #007914

PVcre	Jackson Laboratories	Stock # 008069
$Na_V1.1^{fl/fl}$	UC Davis MMRRC	Stock # 041829-UCD
$MrgprD^{GFP}$	Zheng et al., 2019	
Software and Algorithms		
pClamp 11.2 Software Suite	Molecular Devices	https://www.moleculardevices.com
Image J	Schneider et al. (2012)	https://imagej.nih.gov
Prism 9	Graphpad	https://www.graphpad.com
LabChart	ADInstruments	https://www.adinstruments.com/products/labchart
MATLAB	MathWorks	https://www.mathworks.com
Software, algorithm, custom (MATLAB)	This study	https://github.com/doctheagrif/Current-Clamp-Matlab-Code_O-Neil-DA

Animals. $Pirt^{cre}$ mice were a kind gift from Dr. Xinzhong Dong (Johns Hopkins University). $Rosa26^{Ai14}$ (stock #007914; (Madisen et al., 2010)) and PV^{cre} (stock # 008069) were obtained from Jackson Laboratories. $Na_V1.1^{fl/fl}$ (stock # 041829-UCD) mice were purchased from the UC Davis MMRRC. MrgprD mice were originally published in Zheng et al., 2019. Genotyping was outsourced to Transnetyx. Animal use was conducted according to guidelines from the National Institutes of Health's Guide for the Care and Use of Laboratory Animals and was approved by the Institutional Animal Care and Use Committee of Rutgers University-Newark, UC Davis, and San José State University (*ex vivo* muscle recordings). Mice were maintained on a 12 h light/dark cycle, and food and water was provided *ad libitum*.

Rotarod. To assess motor coordination, a rotarod machine (IITC Life Sciences, Woodland Hills, CA) that has an accelerating rotating cylinder was used. Mice were acclimated to the behavior room for 2 h prior to testing. Mice were assayed on the rotarod for 3 consecutive days, with 3 trials per day and an intertrial interval of at least 15 min. The average of the three trials per day was used. The experimenter was blind to genotype.

Open field test. Mice were acclimated to the behavior room for 2 h prior to testing. The open field apparatus consisted of a black square sound attenuating box of dimensions 40.6 cm × 40.6 cm.

A camera suspended above the arena was connected to a computer running Ethovision XT software, which tracked animal movement and velocity. An animal was placed in the center of the arena and allowed to freely explore for a 10 min trial. The experimenter was blind to genotype.

Tissue processing. For spinal cord immunolabeling experiments, whole spinal columns from adult $Pirt^{Cre}$;$Rosa26^{Ai14}$ and $Pirt^{Cre}$;$Na_V1.1^{fl/fl}$ animals were harvested on ice. For Tdtomato IHC, spinal columns were fixed overnight at 4°C in 4% paraformaldehyde. For vesicular glutamate transporter 1 (VGLUT1) and choline acetyltransferase (ChAT) co-labeling experiments, spinal columns were fixed in 4% paraformaldehyde for 1 h on ice. Tissue was then placed in 30% sucrose solution overnight at 4°C. Following cryoprotection, tissue was embedded in optimal cutting temperature compound (OCT, Tissue-Tek® Sakura) and stored at -80ºC until sectioning. DRG were harvested from thoracic spinal levels and fixed in 4% formaldehyde for 15 min at 4°C and were then incubated in 30% sucrose for 2-4 h at 4°C. DRG were embedded in OCT and stored at -80°C until sectioning.

Immunohistochemistry. Immunohistochemistry of spinal cord cryostat sections (30μm) was performed using the following primary antibodies: Rabbit anti-DsRed (1:3000, Takara Bio, 632496), guinea pig anti-VGLUT1 (1:8000, Zuckerman Institute, 1705), and rabbit anti-ChAT (1:10,000, Zuckerman Institute, 1574). Secondary antibodies used were as follows: anti-rabbit 594 (1:1000, ThermoFisher, A32740), anti-guinea pig 488 (1:1000, ThermoFisher, A11073), and anti-chicken 647 (ThermoFisher, A32733). Specimens were mounted with Fluoromount-G with DAPI (SouthernBiotech, 0100-20). EDL muscles used in *ex vivo* muscle afferent recordings were placed in ice cold 4% paraformaldehyde for 1 h followed by ice cold methanol for 15 min. Muscles were incubated in blocking solution (0.3% PBS-T and 1% BSA) followed by incubation in primary antibodies (guinea pig anti-VGLUT1 1:800 and chicken anti-NFH 1:300, ThermoFisher ab4680)

for 3-6 days at 4ºC. After primary antibody treatment, tissue was washed in blocking solution and treated with secondary antibody (anti-guinea pig 488 1:50 and anti-chicken 594 1:300, Invitrogen, WA316328) for 2-3 days. Specimens were mounted with VECTASHIELD® with DAPI (H-2000, Vector Laboratories). All specimens were imaged in three dimensions on a on a Zeiss LSM880 Airyscan confocal microscope. Images were analyzed using ImageJ software.

Multiplex* in situ *hybridization. Fixed-frozen DRG tissue was cut in 25μm sections and placed on electrostatically coated slides. Sections were processed for RNA *in situ* detection using a modified version of the manufacturer's protocol ((Griffith et al., 2019), Advanced Cell Diagnostics) and the following probes: *Pvalb* (421931- C1, mouse), *Runx3* (451271-C3, mouse), *Scn1a* (556181-C2, mouse). Following *in situ* hybridization, sections were incubated in blocking solution (5% normal goat serum, 0.1% PBS-T) for 1 h at RT. Tissue was then incubated in primary antibodies overnight at 4°C. The following antibodies were used: rabbit DsRed (1:3000, Takara Bio, 632496), rabbit β3-tubulin (1:3000, Abcam, ab18207), chicken β3-tubulin (1:500, Abcam, ab41489), rabbit CGRP (1:1000, Immunostar, 24112), chicken GFP (1:3000, Abcam, ab13970), and chicken NFH (1:3000, Abcam, ab4680). Tissue was treated with the following secondary antibodies for 45 min at RT: anti-rabbit 448 (1:1000, Invitrogen, A32731), 594 (1:1000, Invitrogen, A11037) and 647 (1:1000, Invitrogen, A32733), anti-chicken 488 (1:1000, Invitrogen, A32931) and 594 (1:1000, Invitrogen, A32740). Sections were washed and mounted with Fluoromount-G with DAPI and imaged in three dimensions (2μm axial steps) on an Olympus confocal (LV3000) using a 40X 0.90 NA water objective lens. Images were auto-thresholded and analyzed using ImageJ software.

DRG culture preparation. DRG were harvested from thoracic spinal levels of adult PV^{cre};$Rosa26^{Ai14}$ (6-16 weeks) mice of both sexes and transferred to Ca^{2+}-free and Mg^{2+}-free

HBSS solution (Invitrogen, 14170-112). Upon isolation, processes were trimmed, and ganglia were transferred into collagenase (1.5 mg/mL; Type P, Sigma-Aldrich, 11213865001) in HBSS for 20 min at 37°C followed by TrypLE Express (ThermoFisher, 12605-010) for 3 min with gentle rotation. TrypLE was neutralized with 10% horse serum (heat-inactivated; Invitrogen, 26050-070) and supplemented with culture media (MEM with L-glutamine, Phenol Red, without sodium pyruvate, ThermoFisher, 11095-080), containing 10,000 U/mL Penicillin-streptomycin (ThermoFisher, 15140-122), MEM Vitamin Solution (Invitrogen, 11120-052), and B-27 supplement (ThermoFisher, 17504-044). Serum containing media was decanted and cells were triturated using a fire-polished Pasteur pipette in the MEM culture media described above. Cells were resuspended and triturated using a plastic pipette tip. Cells were plated on glass coverslips that had been washed in 2M NaOH for at least 4 h, rinsed with 70% ethanol, UV-sterilized, and treated with laminin (0.05 mg/mL, Sigma-Aldrich, L2020-1MG) for 1 hour prior to plating. Cells were then incubated at 37°C in 5% CO_2. Cells were used for electrophysiology experiments 14-36 h post-plating.

In Vitro *Electrophysiology.* Whole-cell voltage-clamp recordings were made from TdTomato-expressing dissociated DRG neurons using patch pipettes pulled from Model P-1000 (Sutter Instruments). Patch pipettes had a resistance of 3-6MΩ when filled with an internal solution containing the following (in mM): 140 CsF, 10 NaCl, 1.1 EGTA, .1 $CaCl_2$, 10 HEPES, and 2.5 MgATP, pH with CsOH to 7.2. Seals and whole-cell configuration were obtained in an external solution containing the following (in mM): 145 NaCl, 5 KCl, 10 HEPES, 10 Glucose, 2 $CaCl_2$, 2 $MgCl_2$, pH 7.3 with NaOH, osmolarity ~320mOsm. Series resistance was compensated by 70-80%. To isolate whole-cell sodium currents during voltage clamp experiments, a modified external solution was applied containing the following solution (in mM): 50 NaCl, 95 TEA-Cl, 10 HEPES, 2 $BaCl_2$, 13 glucose, 0.03 $CdCl_2$, pH 7.3 with NaOH, Osmolarity ~320mOsm. Voltage clamp

recordings were performed at room temperature and current clamp recordings were conducted at 37ºC. Bath temperature was controlled and monitored using CL-100 (Warner Instruments).

Ex vivo *electrophysiology*. The effect of the loss of $Na_V1.1$ on muscle spindle afferent firing rates during muscle stretch and sinusoidal vibration was determined using an isolated muscle nerve preparation. The extensor digitorum longus muscle and innervating peroneal branch of the sciatic nerve were dissected from adult (2-4 month old) mice of both sexes. Muscles were held at optimal length (Lo), or the length of the muscle that maximal force of twitch contraction occurred. A series of nine 4 s ramp-and-hold stretches were given to 3 different stretch lengths repeated 3 times each (2.5%, 5%, and 7.5% Lo; ramp speed 40% Lo/s). A series of twelve 9 s sinusoidal vibrations were given (25, 50, and 100 µm amplitude; 10, 25, 50, and 100 Hz frequency). A one-minute rest was given between each length change. Firing rates during a 10 s baseline before stretch (resting discharge or RD) and the maximal firing rate during the ramp up phase of stretch (dynamic peak or DP) were calculated for all animals. We determined whether the response to static stretch was maintained consistently throughout the 4s stretch, as well as the coefficient of variability of the interspike interval (ISI) during the plateau phase of stretch (CV = Std Dev/Mean of ISI over the time period of 1.5-3.5s after end of ramp up). Average firing rate during the 9 s of vibration and whether the unit could entrain in a 1:1 fashion to vibration was also determined. Detailed methods can be found in Wilkinson et al., 2012.

Data acquisition and analysis. Currents and voltages were acquired using pClamp software v11.2 (Molecular Devices). Recordings were obtained using an AxoPatch 200b patch-clamp amplifier and a Digidata 1550B and filtered at 5 kHz and digitized at 10 kHz. Voltage-clamp and current-clamp experiments were analyzed with Clampfit software v11.2 (Molecular Devices) and custom MatLab Scripts. *Ex vivo* recordings were obtained using an A-M Systems Model 1800

extracellular amplifier with headstage and digitized using an ADInstruments PowerLab. Data was analyzed using ADInstruments LabChart software using the Spike Histogram function.

Pharmacology. ICA 121431 was purchased from Tocris Bioscience. All other chemicals were from Sigma-Aldrich and Fisher Chemical.

Experimental design and statistical analysis. Summary data are presented as mean ± SD from *n* cells or afferents, or *N* animals. For quantitative analysis of *in situ* hybridization data, at least 3 biological replicates per condition were used and the investigator was blinded to genotype for analysis. Statistical differences was determine using parametric tests for normally distributed data and non-parametric tests for data that did not conform to Gaussian distributions or had different variances. Statistical tests are listed in *Results* and/or figure legends. Statistical significance in each case is denoted as follows: *p <0.05, **p < 0.01, ***p < 0.001, and ****p < 0.0001. Statistical tests and curve fits were performed using Prism 9.0 (GraphPad Software).

RESULTS

Most studies have found $Na_V1.1$ expression primarily in myelinated sensory neurons that transmit mechanical signals (Fukuoka et al., 2008; Ho and O'Leary, 2011; Wang et al., 2011). In line with prior work, RNAscope analysis of DRG sections from adult mice show that 93% of myelinated neurons, as determined by neurofilament heavy chain (NFH) labeling, expressed $Na_V1.1$ transcripts (**Fig 1A**). RNA-sequencing datasets have consistently identified $Na_V1.1$ expression in proprioceptors; thus, we next analyzed $Na_V1.1$ expression in genetically identified proprioceptors and found 100% of those neurons were positive for $Na_V1.1$ message (**Fig 1B**), consistent with the observation that $Na_V1.1$ protein is expressed in muscle spindle afferents (Carrasco et al., 2017), which innervate proprioceptive end organs found in skeletal muscle. This

contrasted with low expression of $Na_V1.1$ in both calcitonin gene related peptide (CGRP) expressing neurons, which represent peptidergic nociceptors, and non-peptidergic polymodal MrgprD-expressing nociceptors (24% and 3%, respectively, **Fig 1C-D**). The coefficient of variation for the integrated fluorescence density of $Na_V1.1$ transcripts from RNAscope experiments in proprioceptors was 76.5 (**Fig 1E-F**).

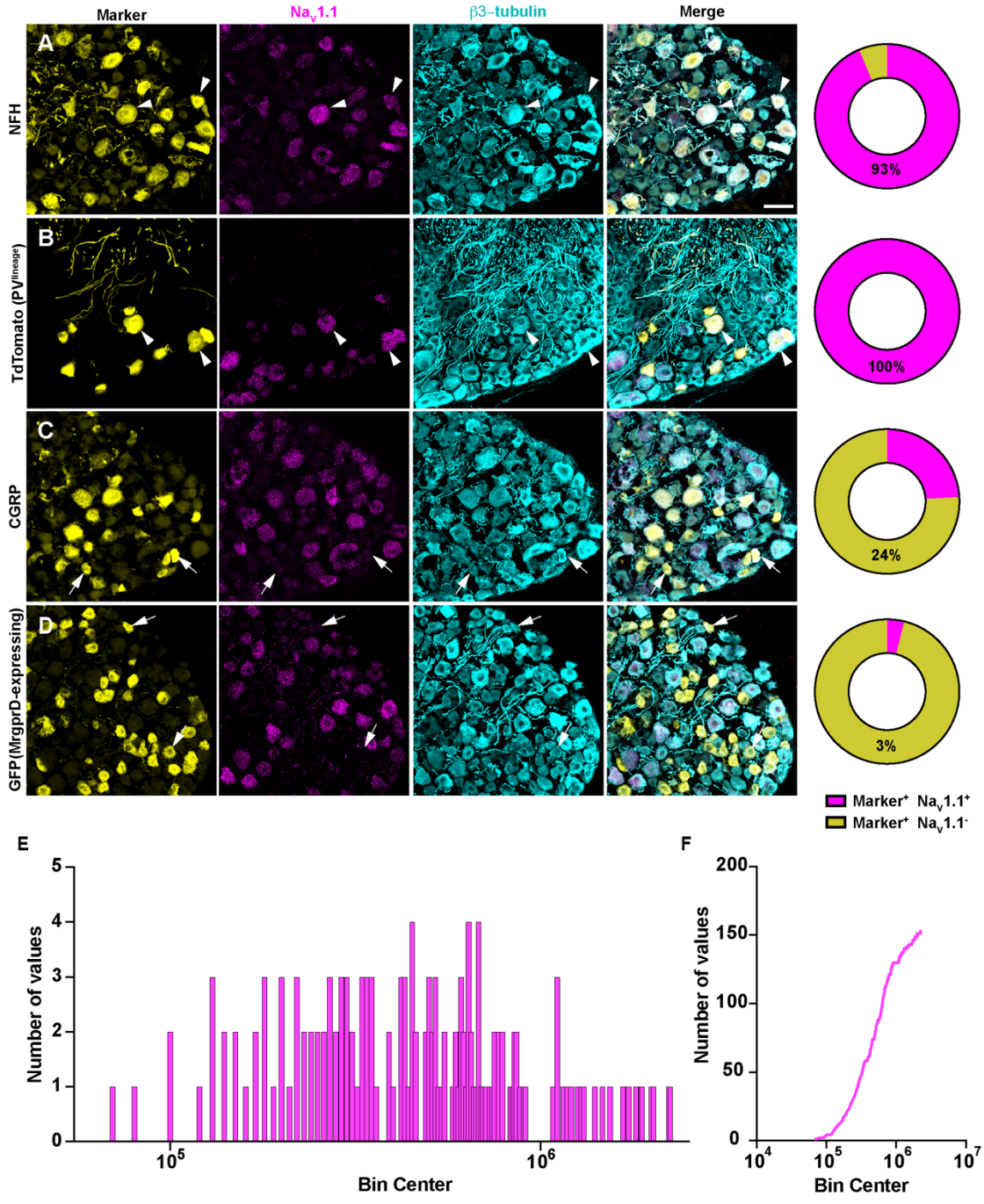

Figure 1. $Na_V1.1$ is ubiquitously expressed in genetically identified proprioceptors. **A-D**, Representative confocal images of cryoprotected adult DRG sections (25 μm) with quantifications indicating the percentage of $Na_V1.1$+ and $Na_V1.1$- neurons in each subpopulation. Images were acquired with a 40X, 0.9 NA water-immersion objective. Sections were hybridized using RNAscope with probes targeting $Na_V1.1$ (*Scn1a*, magenta) and stained with the following antibodies (yellow): (**A**) anti-neurofilament heavy (NFH, n=787) (**B**) anti-DsRed (TdTomato, n=143) (**C**) anti-calcitonin gene-related peptide (CGRP, n=877) (and (**D**) anti-GFP to label MrgprD+ neurons. C57BL/6, $Parvalbumin^{Cre;}Rosa26^{Ai14}$, and $Mrgprd^{GFP}$ DRG we used (n=774). All sections were stained with anti-β3-tubulin (cyan). Scale bar 50μm. White arrowheads indicate $Na_V1.1$+ neurons while white arrows indicate $Na_V1.1$- neurons. Frequency (**E**) and cumulative (**F**) distribution plots of integrated fluorescence density of $Na_V1.1$ in TdTomato+ proprioceptors (n=153) **B**. n = cells.

To determine if $Na_V1.1$ message in proprioceptors is translated into functional surface protein, we performed pharmacological *in vitro* patch clamp experiments from TdTomato+ neurons harvested from $Parvalbium^{Cre}$;$Rosa26^{Ai14}$ (PV^{Ai14}) adult mice (6-15 weeks, N = 10 mice), which represent genetically identifiable proprioceptors harvested from thoracic spinal levels (de Nooij et al., 2013). The $Na_V1.1$ blocker, ICA 121431 (ICA, 500 nM), was used to block $Na_V1.1$. While ICA also blocks $Na_V1.3$, those channels are not expressed in uninjured adult DRG neurons (Chang et al., 2018; Felts et al., 1997; He et al., 2010; Usoskin et al., 2015; Waxman et al., 1994) and RNA-sequencing has not found $Na_V1.3$ message in proprioceptors. In voltage clamp experiments, ICA application reduced the whole-cell sodium current (I_{Na}) on average by 46%, suggesting $Na_V1.1$ is a dominant sodium channel isoform in these neurons (**Fig 2A-B**). I_{Na} density in proprioceptors on average fell from -150 pA/pF to -80 pA/pF following wash on of ICA (**Fig 2C**). I_{Na} had an average decay tau of 0.8 ms in proprioceptors, which was significantly slowed to 1.1 ms following application of ICA (**Fig 2D**). Blocking $Na_V1.1$ also resulted in a moderate but significant slowing of the sodium current rise time from 0.2 ms to 0.3 ms (**Fig 2E**). Quantification of the ICA-sensitive component found an average decay tau of 0.5 ms and an average current density of -89 pA/pF (**Fig 2F**). Of note, there was a wide distribution of current densities for the ICA-sensitive component, ranging from ~-37 pA/pF to ~-168 pA/pF, suggesting some variability in the contribution of $Na_V1.1$ to proprioceptor excitability. As such, we next used current clamp experiments to determine of effect of ICA on proprioceptor action potential firing (**Fig 2G**).

Analysis of current clamp data showed that pharmacological inhibition of $Na_V1.1$ significantly reduced the number of evoked action potentials in most genetically identified proprioceptors (**Fig 2H**); however, of the 20 cells recorded, 5 had low firing rates that were not further inhibited by ICA, indicating in some proprioceptors subtypes other Na_Vs mediate to action potential firing. Action potential amplitude (**Fig 2I**, p = 0.0420) and action potential threshold (**Fig 2J**, p = 0.0186) were also significantly reduced following ICA application. The reduction in action potential threshold is consistent with loss of $Na_V1.1$, which has a V ½ of activation of ~ -15 mV (Aman et al., 2009). We also observed a significant increase in action potential full-width half-max following ICA application (**Fig 2K**, p = 0.0068), in line with loss of the fast $Na_V1.1$-mediated current. To our knowledge, these data are the first reported analysis of the I_{Na} in proprioceptors and identify $Na_V1.1$ as a major contributor.

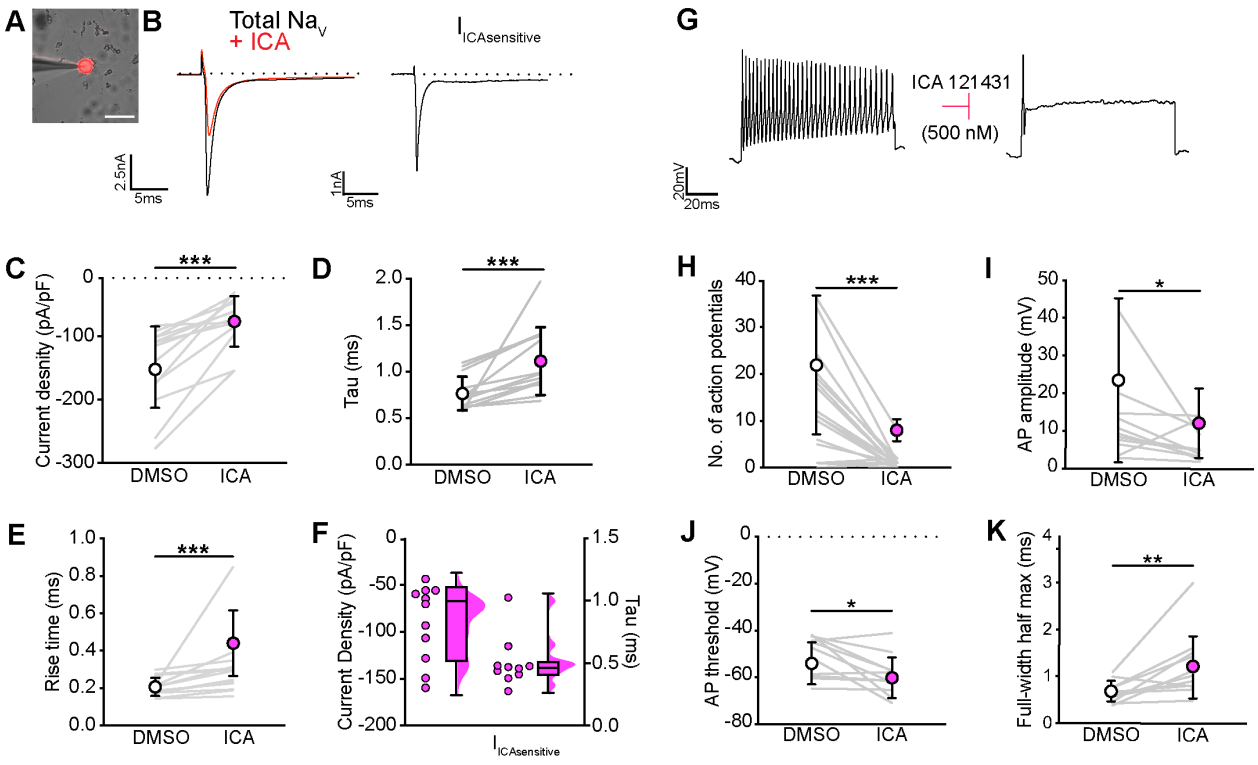

Figure 2. $Na_V1.1$ significantly contributes to the whole-cell sodium current and intrinsic excitability in genetically identified proprioceptors. A. Representative image of a TdTomato-positive proprioceptor in culture during electrophysiological recordings (scale bar set to 50μm). **B.** Left, representative whole-cell voltage-clamp traces

elicited before (black) and after (red) application of ICA121431 (500nM). Right, the subtracted ICA-sensitive current shown in black. **C.** Quantification of the reduction in whole-cell current density before (white) and after (magenta) ICA, p = 0.0002, n=13 cells. **D.** Quantification of rate of current decay before and after ICA, p = 0.0002, n=13 cells. **E.** Quantification of whole-cell current rise time before and after ICA, p = 0.0002, n=13 cells. **F.** Left, current densities of ICA-sensitive sodium currents (n=11), right, current decay taus of ICA-sensitive sodium currents (n=10 cells). **G.** Representative whole-cell current clamp traces before (left) and after (right) application of ICA. **H-K,** Quantification of number of action potentials in response to current injection (**H,** p = 0.0002, n=20 cells), action potential amplitude (**I,** p = 0.0420, n=20 cells), action potential threshold (**J,** p = 0.0186, n=20 cells), and full-width half max (**K,** p = 0.0068, n=20 cells). Grey lines represent paired observations, circles and lines represent means and standard deviations. White circles, before ICA application. The Wilcoxon matched-pairs signed rank test was used to determine significance.

We next sought to determine if $Na_V1.1$ plays an *in vivo* role in motor behaviors. $Na_V1.1$ makes critical contributions to the excitability of parvalbumin-positive interneurons in the brain; thus, we were precluded from using a PV^{cre} driver line to directly interrogate a role for $Na_V1.1$ in proprioceptors, as loss of $Na_V1.1$ in these interneurons produces an epilepsy phenotype that complicates behavioral analyses in adult animals (Ogiwara et al., 2007). As such, we used a $Pirt^{Cre}$ driver to delete $Na_V1.1$ in all sensory neurons to determine the contribution of peripherally expressed $Na_V1.1$ to motor behaviors (Kim et al., 2008). Consistent with *in vitro* data, $Pirt^{Cre}$;$Na_V1.1^{fl/fl}$ ($Na_V1.1^{cKO}$) animals of both sexes displayed profound and visible motor abnormalities. These abnormalities include ataxic-like tremors when suspended in the air (**Supplemental video 1**), abnormal limb positioning (**Supplemental videos 2-3**), and paw clasping, which are absent in $Na_V1.1^{fl/fl}$ littermate controls and heterozygous animals ($Pirt^{Cre}$;$Na_V1.1^{fl/+}$, $Na_V1.1^{Het}$, respectively, **Fig 3A**). We first ran animals in the open field test for ten minutes each to quantify spontaneous locomotor behaviors (**Fig 3B**). We found that $Na_V1.1^{cKO}$ animals traveled significantly less (**Fig 3C**) and slower (**Fig 3D**) than $Na_V1.1^{fl/fl}$ littermate controls (p = 0.0077 and 0.0057, respectively). Surprisingly, $Na_V1.1^{Het}$ mice also displayed motor abnormalities in the open field test, performing similarly to $Na_V1.1^{cKO}$ animals (**Fig 3B-D**), demonstrating $Na_V1.1$ haploinsufficiency in sensory neurons for motor behaviors. No genotype-dependent differences were observed in the amount of time spent moving, suggesting gross motor function was intact (**Fig 3E**). Additionally, the amount of time spent in the center of the open field chamber was also independent of genotype (**Fig 3F**). We next used the rotarod assay to investigate differences in motor coordination. Mice were assayed on three consecutive days and

latency-to-fall and RPM were quantified. Unlike in the open field assay, both $Na_V1.1^{fl/fl}$ and $Na_V1.1^{Het}$ mice performed at similar levels during the three-day period (**Fig G-H**). Conversely, $Na_V1.1^{cKO}$ animals performed significantly worse. By day 3, on average they were only able to maintain their position on the rotarod for 41 s, falling over 50% faster $Na_V1.1^{fl/fl}$ and $Na_V1.1^{Het}$ mice. We did not observe any sex dependent differences in performance in the open field or rotarod tests (**Supplementary Fig 1**). We confirmed that our mouse model selectively targeted sensory neurons by crossing a $Pirt^{Cre}$ driver with a fluorescent reporter line ($Pirt^{Cre}$;$Rosa26^{Ai14}$). We observed little-to-no neuronal expression of TdTomato in both dorsal and ventral spinal cord (**Supplementary Fig 2**). In contrast, DRG neurons somata and axons showed strong labeling. Collectively, our behavioral data provide evidence for a new *in vivo* role of $Na_V1.1$ in sensory neurons in motor behaviors and coordination.

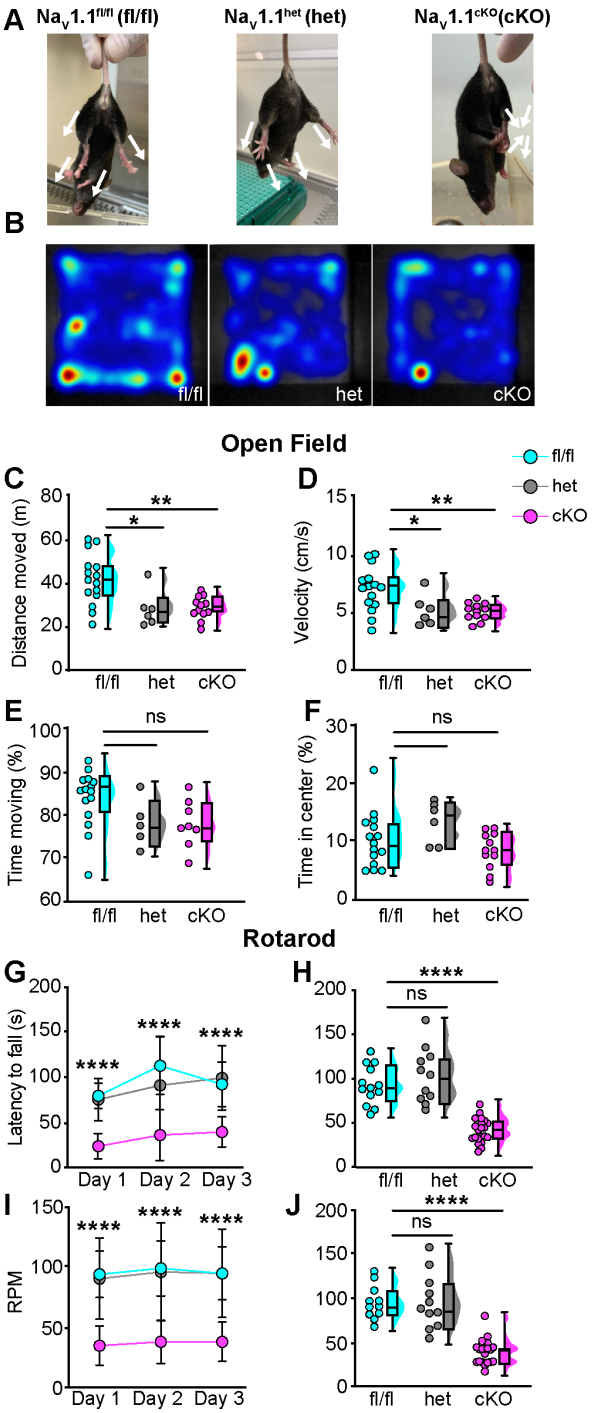

Figure 3. Loss of Nav1.1 in peripheral sensory causes deficits in motor behaviors. A. Representative images showing limb positions of adult Na$_V$1.1$^{fl/fl}$ (left), Na$_V$1.1^{Het} (middle), and Na$_V$1.1^{cKO} (right) mice. White arrows represent the direction of limbs. **B.** Representative heat maps from open field experiments between Na$_V$1.1$^{fl/fl}$ (left), Na$_V$1.1^{Het} (middle), and Na$_V$1.1^{cKO} (right). Open Field (**C-F**), Quantification of total distance traveled during a 10-minute open-field test between Na$_V$1.1$^{fl/fl}$ (cyan), Na$_V$1.1^{Het} (grey), and Na$_V$1.1^{cKO} (magenta) mice (**C,** Na$_V$1.1^{Het} p = 0.0255, Na$_V$1.1^{cKO}, p = 0.0077, compared to Na$_V$1.1$^{fl/fl}$,), average animal velocity (**D,** Na$_V$1.1^{Het} p = 0.00311, Na$_V$1.1^{cKO}, p = 0.0057, compared to Na$_V$1.1$^{fl/fl}$), percent time moving (**E,** Na$_V$1.1^{Het} p = 0.1362, Na$_V$1.1^{cKO}, p = 0.0730, compared to Na$_V$1.1$^{fl/fl}$), and percent time spent in center (**F,** Na$_V$1.1^{Het} p = 0.2297, Na$_V$1.1^{cKO}, p = 0.2494, compared to Na$_V$1.1$^{fl/fl}$) during the test. Rotarod

(**G-I**), Quantification of the latency to fall across three consecutive training days (**G**) and the day-three (**H**). Quantification of revolutions per minute (RPM) at the moment of animal fall (**I**) and the day-three average (**J**). Each dot represents one animal. ****p < 0.0001. A one-way ANOVA (Dunnett's post hoc comparison) was used to determine statistical significance in **C-F** and **I** and **J**. A two-way mixed-design ANOVA (Dunnett's post hoc comparison) was used to determine statistical significance in **G** and **H.** Open field: $Na_V1.1^{fl/fl}$ N=15, $Na_V1.1^{Het}$ N=6, $Na_V1.1^{cKO}$ N=12. Rotarod: $Na_V1.1^{fl/fl}$ N=11, $Na_V1.1^{Het}$ N=11, $Na_V1.1^{cKO}$ N=20.

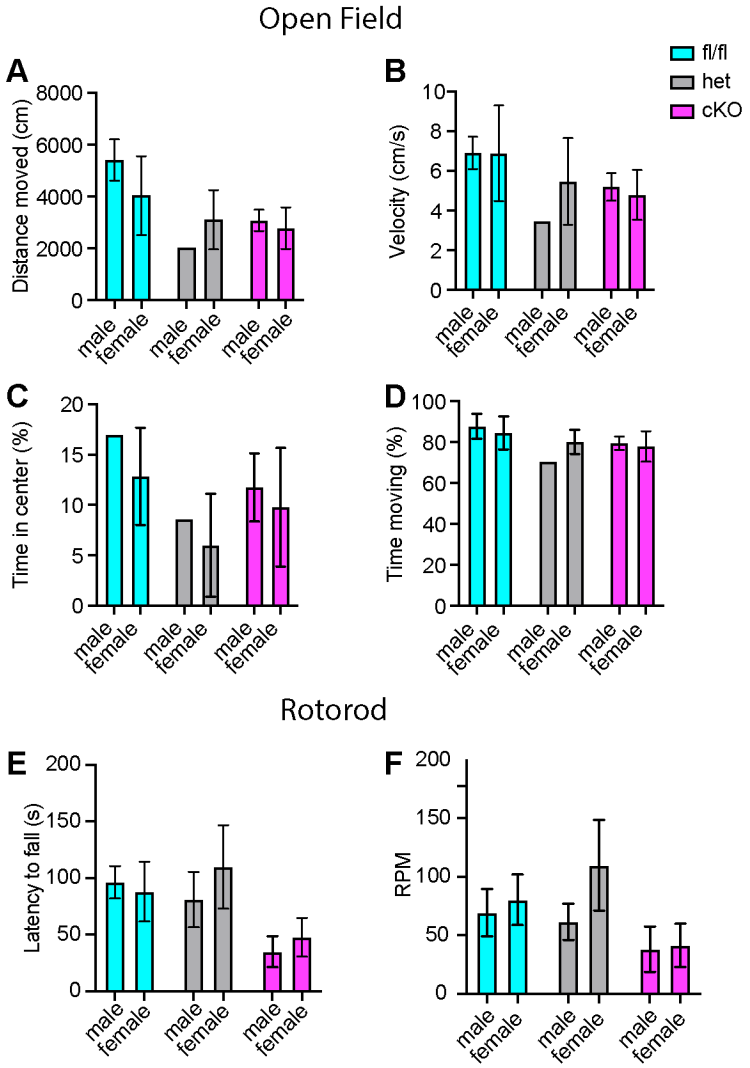

Supplementary Figure 1. Motor deficits in $Na_V1.1^{Het}$ and $Na_V1.1^{cKO}$ animals are not sex dependent. A-D. Quantification of sex-dependent parameters during a 10-minute open field trial. Total distance moved (**A**). Velocity (**B**). Percent time spent in center of box (**C**). Total percent time moving (**D**). Quantification of the sex-dependent differences in rotarod day-three trial latency to fall (**E**) and RPM (**F**).

367

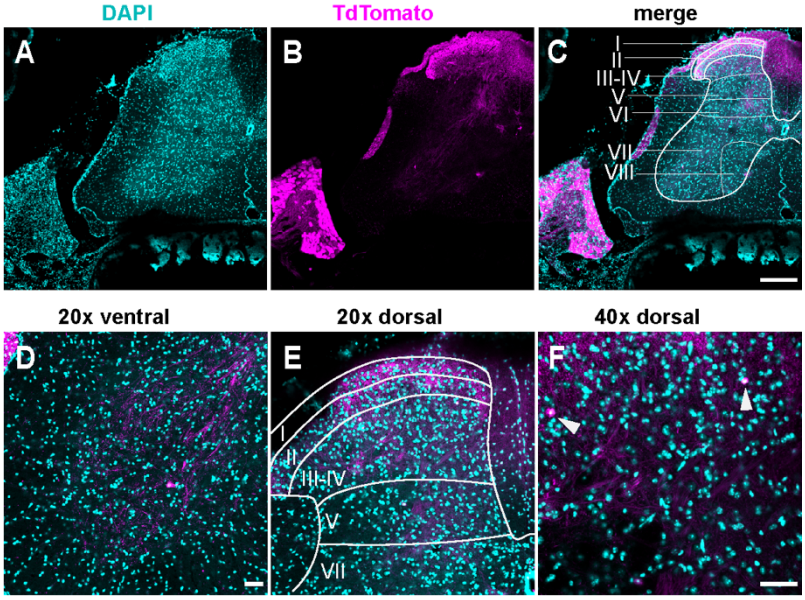

368 **Supplementary Figure 2. TdTomato expression is limited to sensory neurons. A-D**, Images stained using
369 immunohistochemistry with anti-DsRed (TdTomato) (**A-C**) Representative confocal images of spinal cord sections at
370 10X, 0.45 NA dry objective. Scale bar 200μm. (**D**) Image was taken at 20X, 0.8 NA dry objective of the ventral horn.
371 (**E**) Image was taken at 20X, 0.8 NA dry objective of the dorsal horn. Scale bar 50μm. (**F**) Image was taken at 40X, 1.3
372 NA oil-immersion objective. Arrows indicate TdTomato+ puncta. Scale bar 50μm. (N=3, n=30 sections).

373

Supplemental Video 1. Uncoordinated movements in $Na_V1.1^{cko}$ animals. A $Na_V1.1^{cko}$ mouse (left) shows abnormal and spastic movements when suspended in the air. These movements are absent in $Na_V1.1^{fl/fl}$ mice (right).

Supplemental Video 2. Abnormal limb position in $Na_V1.1^{cko}$ animals. A $Na_V1.1^{cko}$ mouse has uncoordinated leg movements and makes an abnormal rotation of its hind paw to grasp its tail while suspended in the air.

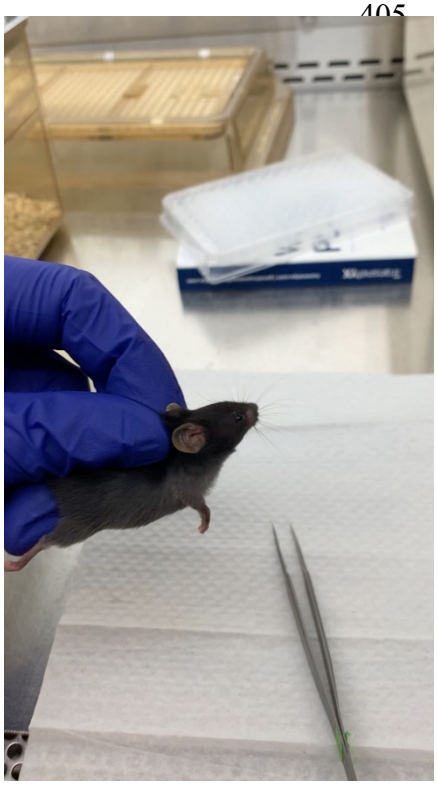

Supplemental Video 3. Abnormal paw position in $Na_V1.1^{cko}$ animals. A $Na_V1.1^{cko}$ mouse is scruffed and places hind paws with foot pads facing down. This contrasts with the normal paw positioning seen in the forepaws, in which foot pads are in the outward facing position.

Pharmacological inhibition of $Na_V1.1$ in proprioceptors *in vitro* significantly reduced intrinsic excitability. Thus, we next asked whether proprioceptor transmission was reduced in $Na_V1.1^{cKO}$ animals. We recorded proprioceptor firing in an *ex vivo* preparation during ramp-and-hold stretch and sinusoidal vibration. Afferents from both $Na_V1.1^{Het}$ and $Na_V1.1^{cKO}$ mice exhibited impaired static stretch sensitivity as evidenced by a decreased likelihood of firing during rest as compared to $Na_V1.1^{fl/fl}$ mice as well as an inability to maintain firing throughout the entire 4s stretch. Almost all afferents from $Na_V1.1^{fl/fl}$ mice could fire consistently throughout the entire 4s hold phase (**Fig 4A**), but loss of one or both copies of $Na_V1.1$ led to either firing only near the beginning of stretch or inconsistent firing in a high percentage of afferents lacking $Na_V1.1$ (**Fig 4B,C**). We quantified this inconsistent firing by determining the coefficient of variation (CV) of the interspike interval (ISI) during the plateau phase of stretch (1.5-3.5 s into the hold phase) across different stretch lengths and found a significant effect of genotype, with the knockout afferents both having higher ISI CV than the $Na_V1.1^{fl/fl}$ afferents (**Fig 4D**; 0.074 ± 0.06, 0.313 ± 0.456, .497 ± .831, at 7.5% Lo, $Na_V1.1^{fl/fl}$, $Na_V1.1^{Het}$, and $Na_V1.1^{cKO}$ afferents, respectively, Two-way ANOVA, $p = 0.015$). In contrast to the clear deficits in static sensitivity in afferents lacking $Na_V1.1$, dynamic sensitivity was not significantly impaired. The maximum firing frequency during the ramp up phase (Dynamic Peak) was independent of genotype, and even trended slightly higher in afferents lacking $Na_V1.1$ (**Fig 4E**; Two-way ANOVA, effect of genotype $p=0.0633$). We next examined the requirement of $Na_V1.1$ for proprioceptor afferent responses to sinusoidal vibration, which were similarly unchanged or enhanced (**Fig 5A-C, Tables 2-4**). We characterized a unit as having entrained to vibration if it fired at approximately the same time every cycle of the 9s vibration. In most cases, afferents lacking Nav1.1 were similarly or more likely to entrain to vibration than $Na_V1.1^{fl/fl}$ afferents (**Fig 5C**). Indeed, $Na_V1.1^{cKO}$ afferents were able to maintain firing during the entire 9 s sinusoidal vibration, in contrast to their inability to maintain consistent firing during static stretch. There were no significant differences in firing rate during vibration between $Na_V1.1^{fl/fl}$,

437 $Na_V1.1^{Het}$, and $Na_V1.1^{cKO}$ afferents. Thus, $Na_V1.1$ is required in proprioceptive afferents for normal

438 responses to static stimuli but is dispensable for afferent responsiveness to dynamic stimuli.

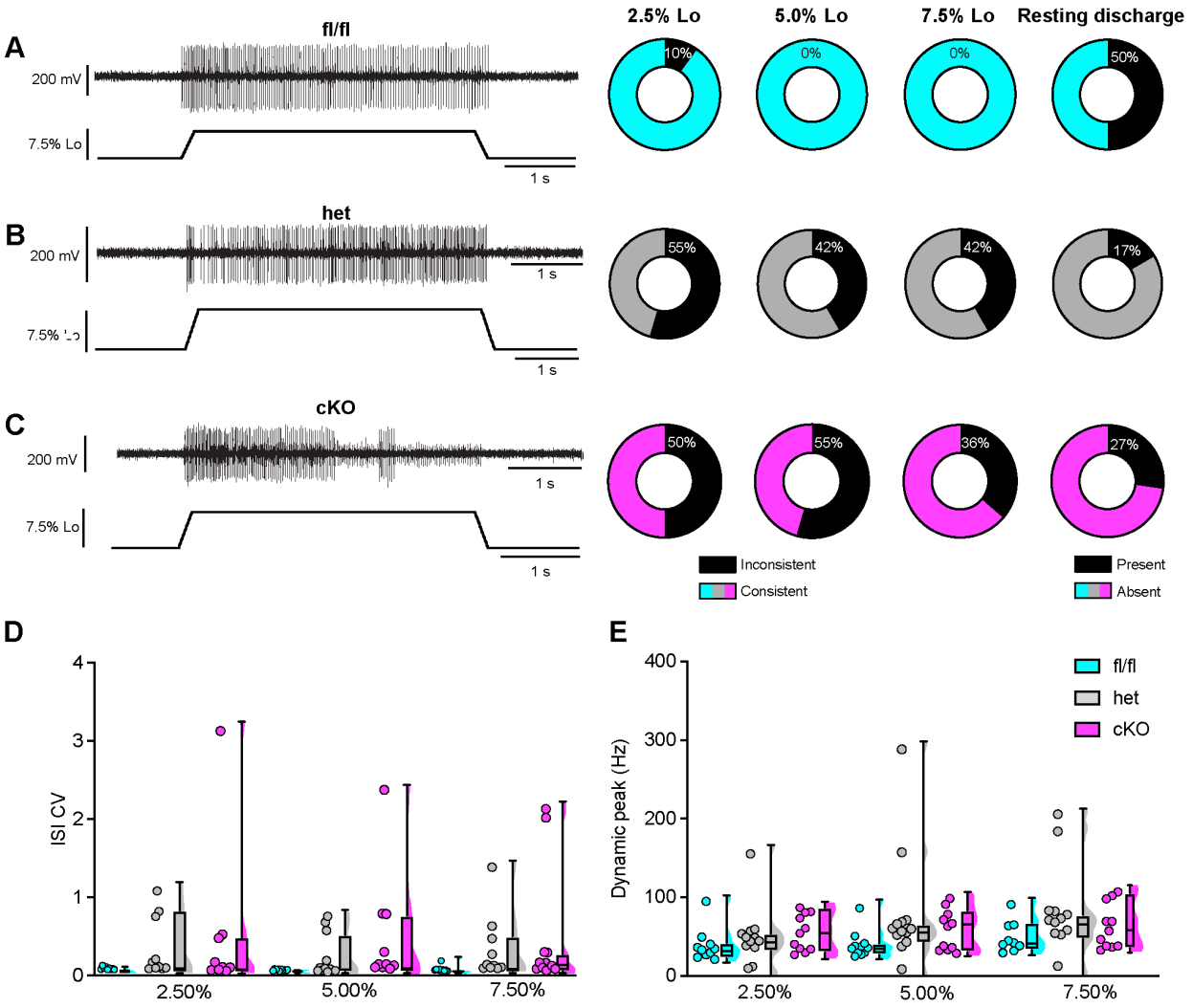

439

440 **Figure 4. Loss of $Na_V1.1$ reduces static muscle stretch sensitivity and reliability. A-C.** Representative responses
441 to ramp-and-hold muscle stretch at 7.5% of Lo from $Na_V1.1^{fl/fl}$ (**A**), $Na_V1.1^{Het}$ (**B**) and $Na_V1.1^{cKO}$ (**C**) afferents. Afferents
442 from $Na_V1.1^{Het}$ and $Na_V1.1^{cKO}$ mice were more likely to show inconsistent firing during the hold phase of stretch. The
443 percentage of afferents from each genotype that were able to fire consistently for the entire duration of stretch at 2.5%,
444 5.0%, and 7.5% of Lo are shown in the pie charts next to the representative trace from their genotype (black indicates
445 percentage with inconsistent firing). The final pie charts represent the proportion of afferents that exhibited resting
446 discharge at Lo for each genotype. **D.** Inconsistency in firing was quantified as the interspike interval coefficient of
447 variation (ISI CV) during the plateau stage of the hold phase of stretch (1.5-3.5s into stretch) for the 3 different
448 genotypes. A significant effect of genotype was observed (two-way mixed-design ANOVA, p=0.015) **E.** The highest
449 firing rate during the ramp up phase of stretch (dynamic peak), which is a measure of dynamic sensitivity. No significant
450 effect of genotype was observed (two-way mixed-design ANOVA, p=0.0633). Each dot represents one afferent
451 ($Na_V1.1^{fl/fl}$, n=10; $Na_V1.1^{Het}$, n=12; $Na_V1.1^{cKO}$, n=11).

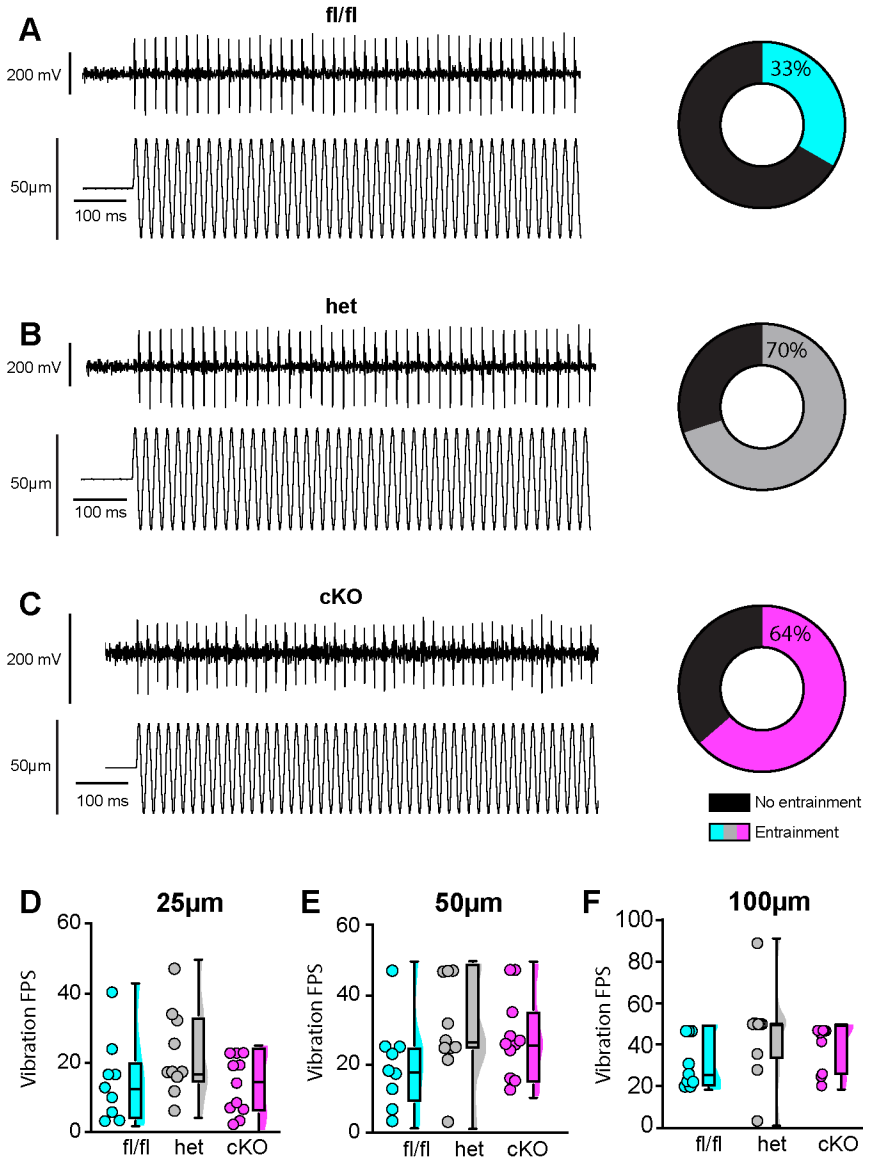

Figure 5. Loss of $Na_V1.1$ does not alter muscle spindle afferent response to vibratory muscle stretch. A-C. Representative traces from afferents that were able to entrain to a 50Hz, 100µm vibration as well as graphs with the percentage of all $Na_V1.1^{fl/fl}$ (cyan; **A**), $Na_V1.1^{Het}$ (gray; **B**), and $Na_V1.1^{cKO}$ (magenta; **C**) afferents that could entrain to the vibration shown in **A-C**. Average firing frequency during a 9 s 50 Hz vibration shown for a 25 µm (**D**), 50 µm (**E**), and 100 µm (**F**) amplitude vibration. There was no significant effect of genotype on the firing frequency during vibration (25 µm, p = 0.2398, 50 µm, p = 0.2413, 100 µm, p = 0.1276). A one-way ANOVA was used to determine statistical significance in **D** and **E**. A Kruskal-Wallis test was used to determine statistical significance in **F**. Each dot represents one afferent ($Na_V1.1^{fl/fl}$, n=9; $Na_V1.1^{Het}$, n=10; $Na_V1.1^{cKO}$,n=11).

Table 2. Afferent entrainment to 25 µm amplitude vibration

Genotype	10 Hz	25 Hz	50 Hz	100 Hz
$Na_V1.1^{fl/fl}$	33.33%	11.11%	0.00%	0.00%
$Na_V1.1^{het}$	50.00%	40.00%	10.00%	10.00%

$Na_V1.1^{cKO}$	27.27%	9.09%	0.00%	0.00%

Table 2. The percentage of muscle spindle afferents that entrained to a 25μm amplitude sinusoidal vibration.

Table 3. Afferent entrainment to 50 μm amplitude vibration

Genotype	10 Hz	25 Hz	50 Hz	100 Hz
$Na_V1.1^{fl/fl}$	88.89%	22.22%	11.11%	11.11%
$Na_V1.1^{het}$	80.00%	70.00%	30.00%	10.00%
$Na_V1.1^{cKO}$	45.45%	54.55%	18.18%	0.00%

Table 3. The percentage of muscle spindle afferents that entrained to a 50μm amplitude sinusoidal vibration.

Table 4. Afferent entrainment to 100 μm amplitude vibration

Genotype	10 Hz	25 Hz	50 Hz	100 Hz
$Na_V1.1^{fl/fl}$	100.00%	44.44%	33.33%	22.22%
$Na_V1.1^{het}$	90.00%	90.00%	70.00%	40.00%
$Na_V1.1^{cKO}$	63.64%	72.73%	63.64%	18.18%

Table 4. The percentage of muscle spindle afferents that entrained to a 100μm amplitude sinusoidal vibration.

Could reduced and inconsistent transmission of static stimuli in proprioceptors lead to a concomitant activity-dependent reduction in the number of mature proprioceptors? To address this question, we performed RNAscope analysis of DRG sections from $Na_V1.1^{fl/fl}$, $Na_V1.1^{Het}$, and $Na_V1.1^{cKO}$ mice. We quantified the number of neurons per DRG section that were positive for both Runx3 and parvalbumin transcript, the molecular signature of mature proprioceptors (**Fig 6**, Oliver et al., 2021). We found no significant genotype-dependent differences in the number of proprioceptors in $Na_V1.1^{Het}$ and $Na_V1.1^{cKO}$ mice compared to $Na_V1.1^{fl/fl}$ controls ($p = 0.3824$ and $p = 0.1665$, respectively), indicating that the behavioral deficits observed in $Na_V1.1^{cKO}$ mice are not the result of a developmental loss of proprioceptors. We also analyzed muscle spindle morphology to determine if aberrant sensory end organ development may contribute to the motor abnormalities of $Na_V1.1^{cKO}$ mice. Similar to conditional Piezo2-knockout animals (Woo et al., 2015), no qualitative differences were observed between genotypes (**Supplementary Fig 3**).

485 Thus, abnormal proprioceptor development does not contribute to the overall phenotype of
486 $Na_V1.1^{cKO}$ mice.

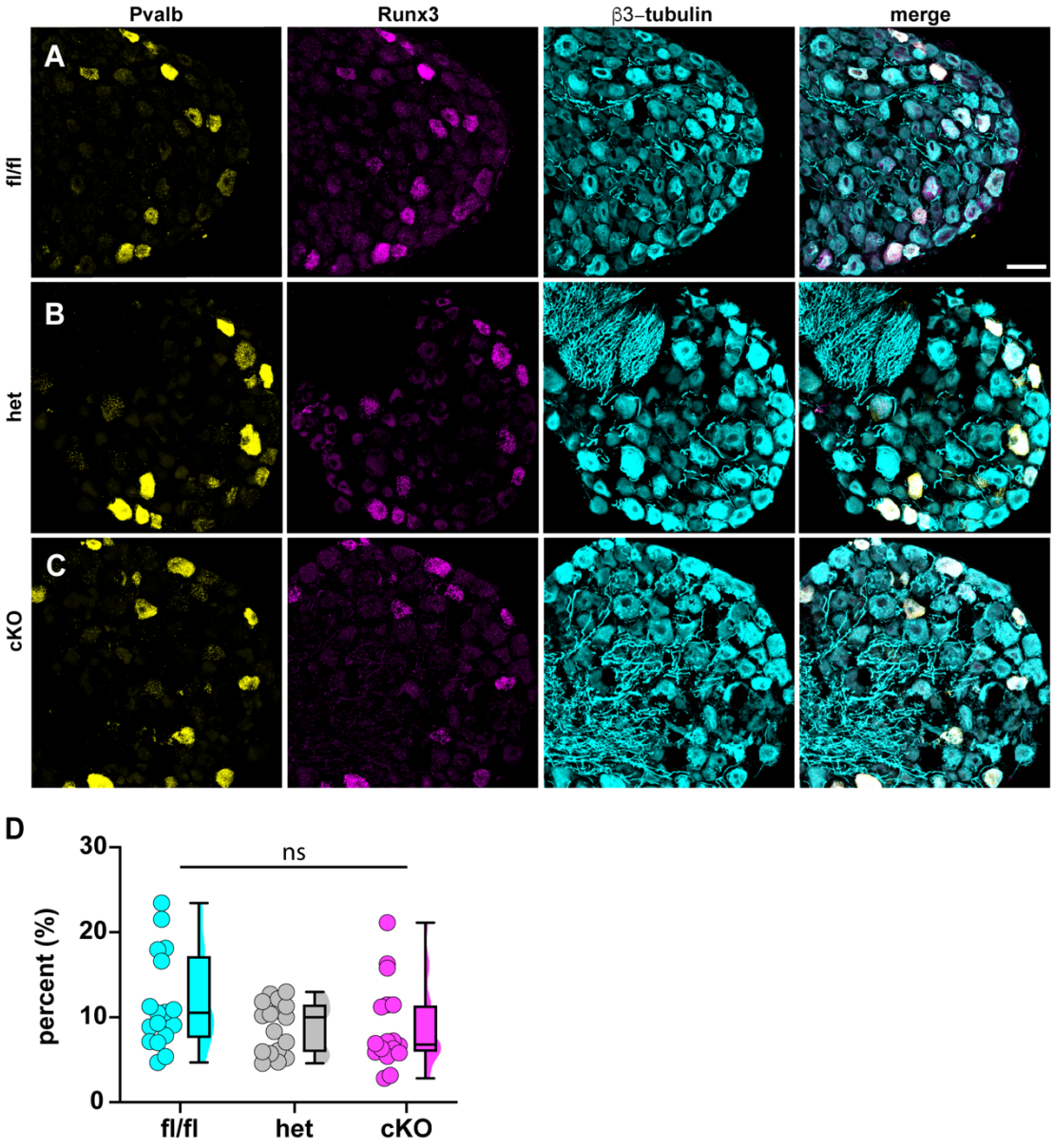

487

488 **Figure 6. Loss of $Na_V1.1$ in sensory neurons does not affect proprioceptor development**. Representative images
489 of $Na_V1.1^{fl/fl}$(**A**), $Na_V1.1^{het}$ (**B**), and $Na_V1.1^{cKO}$ (**C**) adult DRG neuron sections (25 μm). Images were acquired with a
490 40X, 0.9 NA water-immersion objective. Sections were hybridized with probes targeting parvalbumin (*Pvalb*, yellow)
491 and *Runx3* (magenta) and immunostained with anti-β3-tubulin (cyan). (**D**) Quantification of the percentage of
492 Pvalb+/Runx3+ neurons in each genotype. Each dot represents one DRG section. A Kruskal-Wallis test with Dunn's
493 post hoc comparison was used to determine statistical significance (p = 0.1971, $Na_V1.1^{fl/fl}$ n=17, $Na_V1.1^{Het}$ n=17,
494 $Na_V1.1^{cKO}$ n=18)). Scale bar 50μm.
495

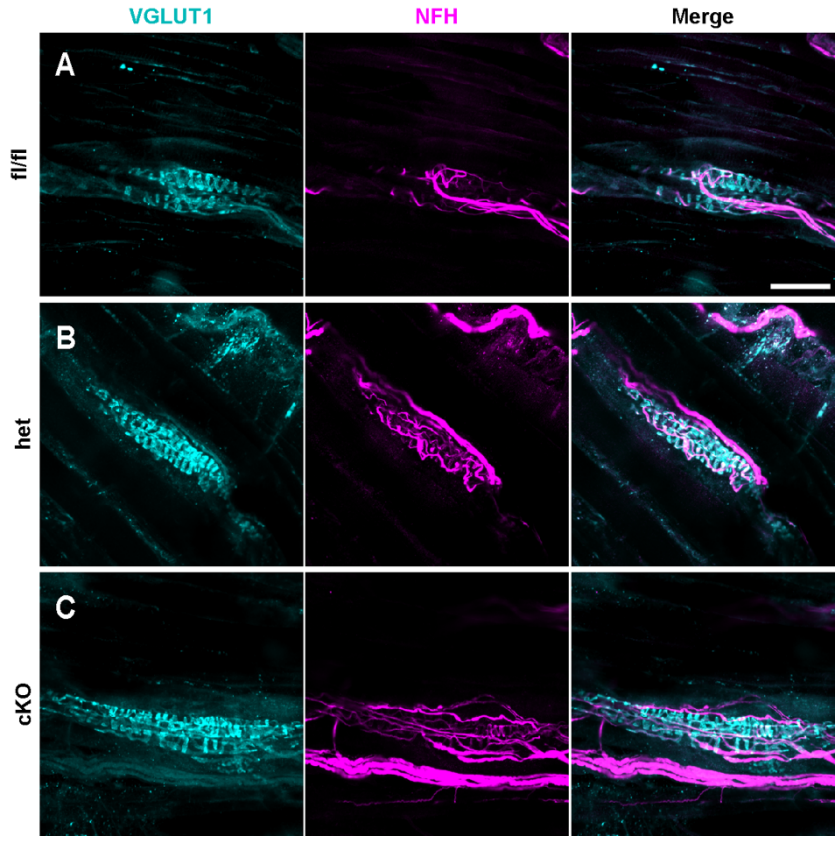

Supplementary Figure 3. Muscle spindle development is normal in $Na_V1.1^{Het}$ and $Na_V1.1^{cKO}$ animals. **A-C**, Representative confocal images of muscle spindle whole mounts. Images were acquired with a 40x, 1.3 NA oil-immersion objective. Sections were stained using immunohistochemistry with VGLUT1 (cyan) and neurofilament heavy (NFH, magenta). (**A**) Representative images from $Na_V1.1^{fl/fl}$ (**B**) $Na_V1.1^{het}$ and (**C**) $Na_V1.1^{cKO}$ mice. $Na_V1.1^{fl/fl}$, n=7,; $Na_V1.1^{Het}$, n=8; $Na_V1.1^{cKO}$, n=9. Scale bar 50μm. n = muscle spindles.

We next asked whether reduced proprioceptor signaling decreased synaptic connectivity between proprioceptive axons and motor neurons in the spinal cord. Spinal cord sections were harvested from $Na_V1.1^{fl/fl}$, $Na_V1.1^{Het}$, and $Na_V1.1^{cKO}$ mice and stained with antibodies against vesicular glutamate transporter 1 (VGLUT1) and choline acetyltransferase (ChAT), to label proprioceptor axons and α- motor neurons in the ventral horn, respectively. Our analysis found a significant decrease in VGLUT+ puncta per ChAT+ motor neuron in $Na_V1.1^{cKO}$ mice compared to $Na_V1.1^{fl/fl}$ littermate controls (**Fig 7,** p = 0.0031). $Na_V1.1^{Het}$ mice showed no significant alterations in connectivity between VGLUT1+ proprioceptive terminals and ChAT+ motor neuron compared to $Na_V1.1^{fl/fl}$ littermate controls (p = 0.7695). Thus, in addition to decreased proprioceptive

512 transmission, $Na_V1.1^{cKO}$ mice also have reduced proprioceptor innervation of motor neurons,
513 suggesting their behavioral deficits may also be due in part to aberrant signaling in the spinal
514 cord.
515

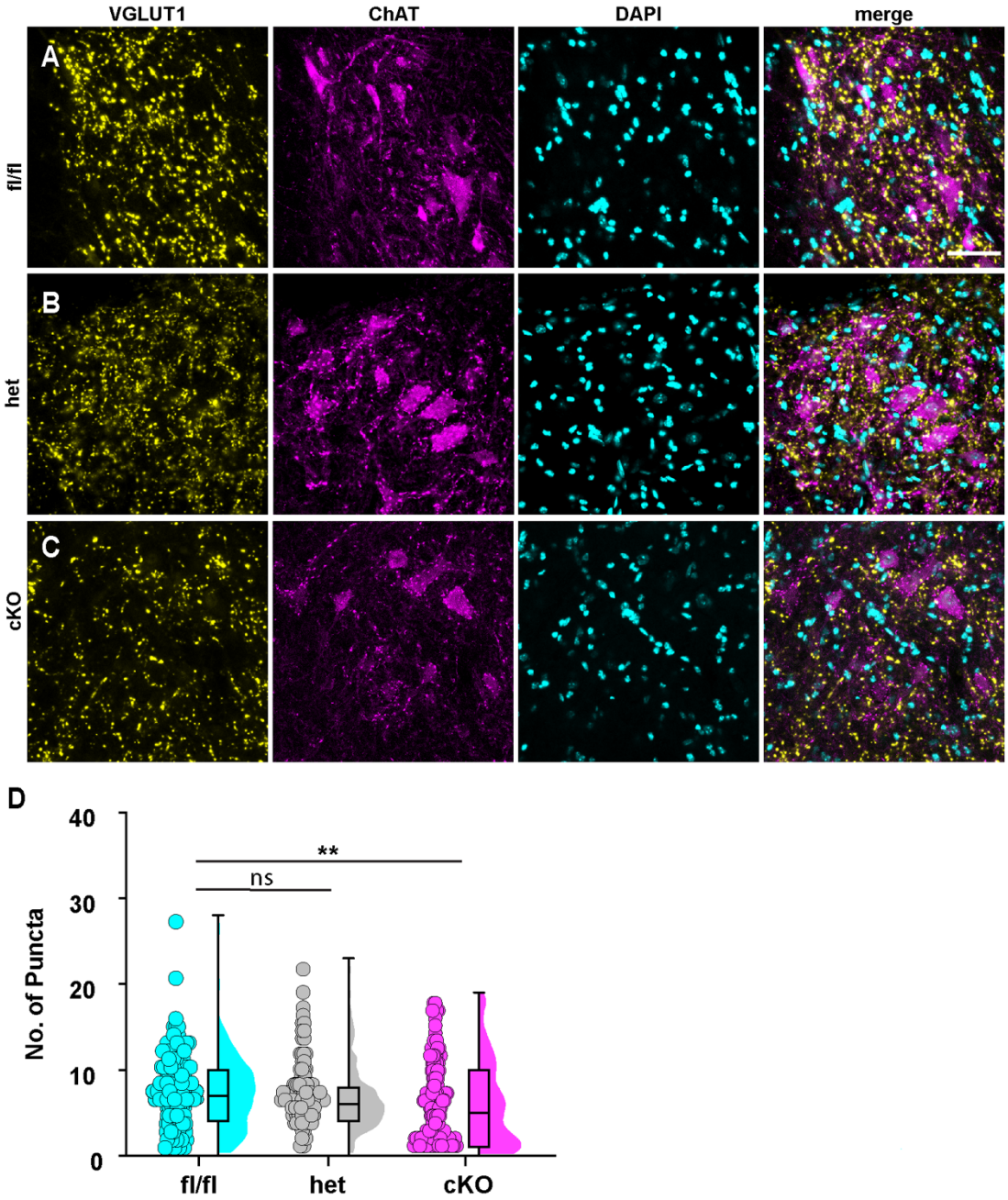

516

517 **Figure 7. Synaptic connectivity is reduced between proprioceptors and a-motor neurons in spinal cords of**
518 **$Na_V1.1^{cKO}$ mice**. **A-C**, Representative images of $Na_V1.1^{fl/fl}$(**A**), $Na_V1.1^{het}$ (**B**), and $Na_V1.1^{cKO}$ (**C**) adult spinal cord sections

(30 μm). Images were acquired with a 63X, 1.4 NA oil-immersion objective. Sections were stained using immunochemistry with VGLUT1 (yellow) and ChAT (magenta). (**D**) Quantification of the number of VGLUT1+ puncta onto ChAT+ motor neurons. A Kruskal-Wallis test with Dunn's post hoc comparison was used to determine statistical significance ($Na_V1.1^{Het}$, p=0.7695, $Na_V1.1^{cKO}$, p=0.0031) Each dot represents a motor neuron. $Na_V1.1^{fl/fl}$, n=127; $Na_V1.1^{Het,}$ n=99; $Na_V1.1^{cKO}$, n=119. Scale bar 50μm. n = cells

DISCUSSION

The critical role for $Na_V1.1$ in various brain disorders has overshadowed the potential contributions of this channel in peripheral signaling. The results presented in this study are the first to provide functional evidence that $Na_V1.1$ in peripheral sensory neurons is required for normal motor behaviors. We found that mice lacking $Na_V1.1$ in sensory neurons exhibit visible motor deficits and ataxic-like behaviors, which were quantified in the rotarod and open field behavioral assays. We propose that this aberrant motor behavior is largely attributed to loss of $Na_V1.1$ in proprioceptors. Indeed, RNAscope analysis showed expression of $Na_V1.1$ mRNA in 100% of parvalbumin-positive DRG neurons. In line with this finding, our functional *in vitro* patch-clamp experiments show pharmacological inhibition of $Na_V1.1$ in proprioceptors is sufficient to significantly attenuate action potential firing, likely due to $Na_V1.1$ carrying nearly half of the I_{Na} in these cells. At the afferent level $Na_V1.1^{cKO}$ and $Na_V1.1^{Het}$ animals show clear deficits in static stretch sensitivity, but not dynamic sensitivity, and could even entrain to vibrations as fast as 100 Hz, suggesting that $Na_V1.1$ in proprioceptors is dispensable for encoding dynamic stimuli. Finally, we found that loss of $Na_V1.1$ in sensory neurons had no effect on proprioceptor development or muscle spindle morphology; however, we did observe a significant reduction in proprioceptive afferent innervation of ChAT+ motor neurons in the spinal cord. Thus, the observed motor deficits are likely due to a combination of reduced static sensitivity of proprioceptor afferents and a concomitant activity-dependent loss of motor neuron innervation.

Our model proposes that $Na_V1.1$ is tasked with maintaining consistent firing in proprioceptors during static muscle stretch for normal motor behaviors, whereby activation of the mechanotransduction channel Piezo2 initiates electrical signaling, which in turn activates a complement of tetrodotoxin-sensitive Na_V channels (Carrasco et al., 2017; Florez-Paz et al., 2016;

548 Woo et al., 2015, **Fig 8**). During dynamic or vibratory stimuli, Piezo2, and likely a combination of
549 other molecular mediators, including $Na_V1.6$ and $Na_V1.7$, are sufficient to elicit normal electrical
550 activity. Conversely, during prolonged muscle stretch when Piezo2 channels presumably
551 inactivate, $Na_V1.1$ is required for regular and reliable firing. In the absence of functional $Na_V1.1$
552 channels, inconsistent proprioceptor firing leads to a decrease in synaptic connectivity in the
553 spinal cord between proprioceptors and motor neurons, likely exacerbating motor deficits. While
554 other signaling molecules and channels, such as vesicle-released glutamate (Bewick et al., 2005;
555 Than et al., 2021), and mechanosensitive ASIC channels (Lin et al., 2016) and ENaC channels
556 (Bewick and Banks, 2015), also contribute to mammalian proprioception, our data suggests
557 $Na_V1.1$ is a critical for muscle spindle mechanotransduction, given the overt behavioral deficits
558 observed in $Na_V1.1^{cKO}$ mice.

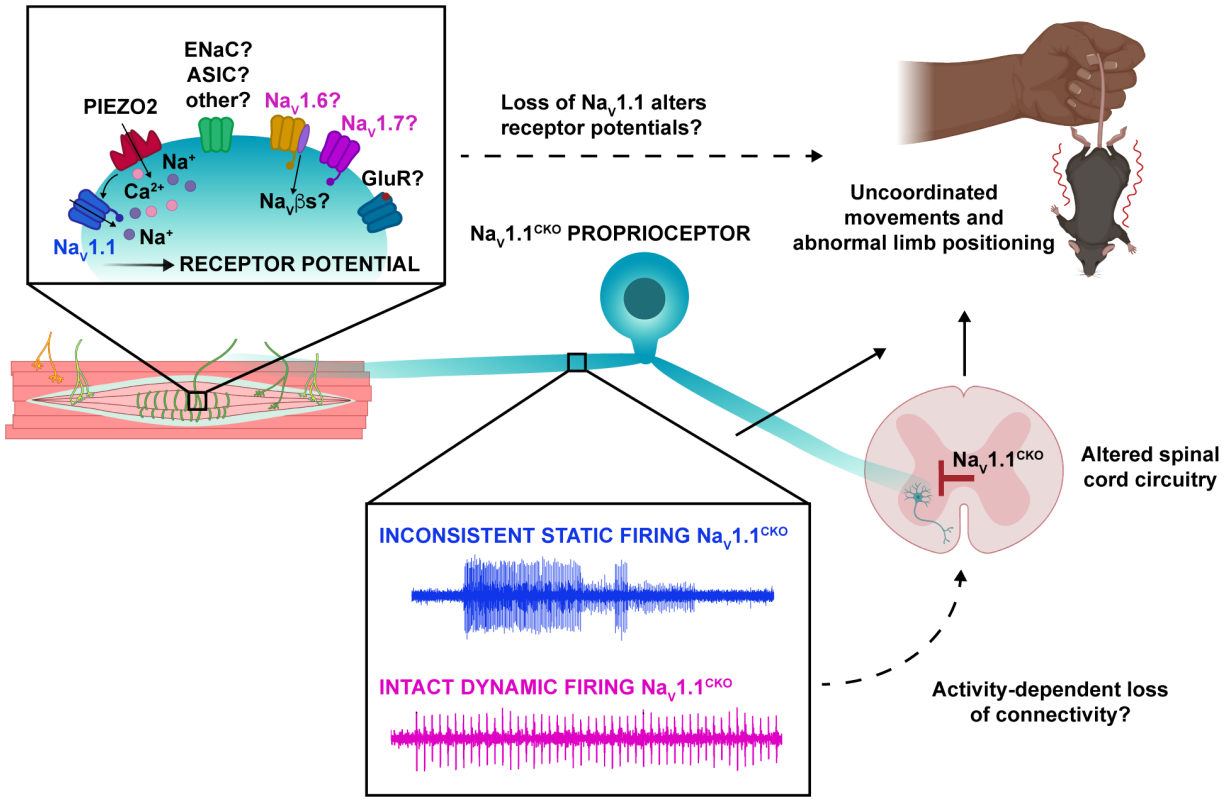

559

560 **Figure 8. Proposed model of the role of $Na_V1.1$ in proprioception.** Upon muscle static stretch, various channels
561 activate, including Piezo2 (red) which results in an influx of calcium and sodium ions, causing a depolarization that
562 activates $Na_V1.1$ (dark blue). $Na_V1.1$ activation drives reliable repetitive firing of proprioceptors during static stretch for
563 normal motor behavior. Loss of $Na_V1.1$ in sensory neurons results in inconsistent static firing at the afferent level while

maintaining dynamic firing. It is possible that a combination of Piezo2, $Na_V1.6$ (yellow) , $Na_V1.7$ (pink), and/or other channels, such as glutamate receptors, Asic channels, and ENaC, mediate dynamic firing. Unreliable signaling may alter spinal cord circuitry through an activity-dependent loss of synaptic connectivity, resulting in uncoordinated movements and abnormal limb positioning.

To date, our knowledge of the functional contributions of $Na_V1.1$ in the PNS is limited. Most studies have identified roles for this channel in mechanical pain signaling in DRG, TG, and vagal sensory neurons. Intraplantar pharmacological activation of $Na_V1.1$ induces spontaneous pain behaviors and mechanical pain, which is absent in mice lacking $Na_V1.1$ in small- and medium-diameter sensory neurons (Osteen et al., 2016). Inhibition of $Na_V1.1$ prevented the development of mechanical pain in several preclinical models, including spared nerve injury (Salvatierra et al., 2018b), an irritable bowel syndrome mouse model (Salvatierra et al., 2018), and infraorbital nerve chronic constriction injury (Pineda-Farias et al., 2021). Additionally, blocking $Na_V1.1$ channels inhibited firing in TRPM8-expressing neurons *in vitro*, suggesting a potential role for this channel in thermosensation (Griffith et al., 2019). No prior studies, however, have reported a role for $Na_V1.1$ in proprioceptor function or motor behaviors.

The biophysical properties of $Na_V1.1$ within the mammalian muscle spindle may help drive static stretch induced action potential firing in proprioceptors. Indeed, the loss of consistent firing we observed during static stretch in $Na_V1.1^{cKO}$ animals is functionally similar to loss of $Na_V1.1$ in other brain cell types. Loss of a single copy of $Na_V1.1$ is sufficient to attenuate sustained action potential firing in parvalbumin-positive hippocampal interneurons (Ogiwara et al., 2007; Yu et al., 2006) and cerebellar Purkinje neurons (Yu et al., 2006). Mechanistically, $Na_V1.1$ might contribute to sustained firing in two distinct ways. First, $Na_V1.1$ has been associated with persistent sodium current ($I_{Na}P$) and resurgent sodium current ($I_{Na}R$), both of which promote repetitive firing in a wide variety of cell types in the CNS and PNS (Barbosa et al., 2015; Kalume et al., 2007; Khaliq et al., 2003). Second, $Na_V1.1$ recovers rapidly from fast inactivation compared to other channel subtypes (Herzog et al., 2003; Patel et al., 2015) and has been shown to be refractory to entry into slow inactivation in TRPM8-expressing DRG neurons (Griffith et al., 2019). Thus, it is possible

that proprioceptors rely on these features of $Na_V1.1$ for reliable and consistent firing in response to static stretch.

Loss of $Na_V1.1$ notably impacted proprioceptor afferent static sensitivity during ramp-and-hold stretch, but not dynamic sensitivity as measured by entrainment to sinusoidal vibrations using *ex vivo* muscle-nerve recordings. Afferents from $Na_V1.1^{cKO}$ animals were more likely to have failures and thus were mostly unable to fire consistently throughout the 4 s of stretch, which was accompanied by a higher coefficient of variability in the ISI. This is consistent with $Na_V1.1$ playing a critical role in transmitting static stretch information to the central nervous system. Interestingly, however, dynamic sensitivity in these afferents appears to be enhanced, or at least unimpaired. Though not statistically significant, $Na_V1.1^{cKO}$ afferents were more likely to entrain throughout the entire 9 s vibration compared to control mice. Therefore, $Na_V1.1^{cKO}$ afferents don't have a generalized inability to maintain high frequency firing, but a more specific deficit in static sensitivity. $Na_V1.1$ has been localized to muscle spindle afferent endings (Carrasco et al., 2017) and has been hypothesized to help amplify receptor current. Our results support a model whereby current via Piezo2 and potentially other mechanically sensitive ion channels at the start of stretch produces a sufficient receptor potential to generate firing at the heminode, but that amplification of the receptor potential by $Na_V1.1$ is necessary to maintain firing during held stretch. A similar deficit in static but not dynamic sensitivity was seen following loss of synaptic-like vesicle released glutamate from afferent endings (Than et al., 2021); however in those afferents firing only occurred at the beginning of stretch and patchy firing was never observed. This may indicate that glutamate plays a more general role maintaining excitability, whereas $Na_V1.1$ is required for reliable action potential generation at heminodes during static stimuli. Alternatively, or in addition, $Na_V1.1$ expressed along the axon could be essential for sustained static firing. A detailed examination of $Na_V1.1$ subcellular localization along proprioceptor afferents could shed light on how this channel contributes to signal propagation. The observed trend towards increased

dynamic sensitivity, especially in $Na_V1.1^{Het}$ animals, could suggest the upregulation of other Na_V subtypes or other molecules as a compensatory mechanism to counteract the loss of $Na_V1.1$. Future studies using temporally controlled deletion of $Na_V1.1$ in sensory neurons could tease this apart. Nevertheless, as static sensitivity is still very much impaired in $Na_V1.1^{cKO}$ afferents, Nav1.1 may play a potentially unique role in maintaining afferent firing during the sustained stretch.

Although though the response patterns of $Na_V1.1^{Het}$ and $Na_V1.1^{cKO}$ afferents were similar, behavioral deficits were much more striking in $Na_V1.1^{cKO}$ mice (**Fig 4**). One potential explanation is the significant decrease in Group Ia proprioceptor synapses (VGLUT1+) on α-motor neurons observed in $Na_V1.1^{cKO}$ animals but not in $Na_V1.1^{Het}$ mice. Nerve injury can permanently reduce VGLUT1 synapses on motor neurons (Alvarez et al., 2011), suggesting they may be particularly sensitive to changes in excitability. Given the similar deficits in static stretch sensitivity between these two genotypes, however, it is unclear why $Na_V1.1^{Het}$ mice maintain normal synaptic connectivity between proprioceptive afferents and α-motor neurons. $Na_V1.1^{Het}$ afferents trended toward having increased dynamic sensitivity, making it is possible that this is sufficient to protect from an activity-dependent loss of motor neuron innervation. Another explanation is a presynaptic role of $Na_V1.1$ in proprioceptive terminals that is unveiled when both copies of $Na_V1.1$ are lost. For example, loss of presynaptic $Na_V1.7$ channels in the spinal cord reduced glutamate release from nociceptive afferents onto dorsal horn neurons (MacDonald et al., 2021). If a similar mechanism is at play for $Na_V1.1$ in proprioceptors, reduced release from afferent terminals could lead to homeostatic changes in connectivity with post-synaptic motor neurons. Future studies are required to test this possibility.

We observed effects of both pharmacological inhibition and genetic deletion of $Na_V1.1$ in *in vitro* and *ex vivo* electrophysiological experiments, respectively (**Figs 2-3, 5**); however, in our mouse model $Na_V1.1$ is deleted in all sensory neurons. Thus, we cannot rule out that loss of $Na_V1.1$ in other mechanosenory neuron populations contributes to the motor deficits observed.

642 Deletion of $Na_V1.1$ in small- and medium-diameter DRG neurons did not produce visible motor
643 deficits (Osteen et al., 2016), indicating sensory neuron populations in those categories are not
644 involved. We did observe $Na_V1.1$ transcripts in the vast majority of myelinated DRG neurons (a
645 combination of large- and medium-diameter DRG neurons), consistent with its presence in
646 different subclasses of tactile sensory neurons (Zheng et al., 2019). However, the severe motor
647 phenotype of $Na_V1.1^{cKO}$ mice precludes mechanical threshold analysis using von Frey or tactile
648 sensitivity using tape test. Notably, baseline mechanical thresholds were unchanged following
649 intraplantar injection of a selective $Na_V1.1$ inhibitor (Salvatierra et al., 2018). This suggests that
650 while $Na_V1.1$ mRNA is expressed in most tactile sensory neurons, functional protein may only be
651 upregulated in these populations during pathological states.

652 Despite this limitation, one noteworthy and intriguing finding from our study was the
653 haploinsufficiency of $Na_V1.1$ in sensory neurons for normal motor behavior in the open field test.
654 $Na_V1.1^{Het}$ mice had an identical phenotype to $Na_V1.1^{cKO}$ mice, moving more slowly and less than
655 controls, despite not having the more severe and visible motor coordination deficits. Indeed, their
656 performance on the rotarod was identical to that of $Na_V1.1^{fl/fl}$ controls. The gene encoding $Na_V1.1$,
657 *Scn1a*, is a super culprit gene with over one thousand associated disease-causing mutations,
658 most of which are linked to different forms of epilepsy. Many epilepsy patients with hemizygous
659 $Na_V1.1$ loss-of-function display ataxia and motor delays and deficiencies (Claes et al., 2001;
660 Fujiwara et al., 2003), which has traditionally been attributed to loss of $Na_V1.1$ function in the
661 brain, namely the cerebellum (Kalume et al., 2007). Our findings suggest that some of the clinical
662 manifestations associated with epilepsy are not solely due to $Na_V1.1$ loss-of-function in the brain,
663 but also may manifest in part as a result from unreliable coding by peripheral proprioceptors.

664 Data presented in this study provide new evidence of a role for peripherally expressed
665 $Na_V1.1$ in motor coordination. We show that $Na_V1.1$ is ubiquitously expressed in mammalian
666 proprioceptors, contributes to proprioceptor excitability *in vitro* and *ex vivo,* and is required in

667 sensory neurons for normal spinal cord motor circuit development. Collectively, this works
668 identifies a new role for $Na_V1.1$ in peripheral sensory neuron physiology and motor behaviors.
669
670 **AUTHOR CONTRIBUTIONS**
671 CME performed immunohistochemistry and voltage-clamp experiments. CML performed
672 RNAscope experiments. SO performed *ex vivo* electrophysiology experiments. MSD performed
673 behavioral experiments. KMW and DAO performed current clamp experiments. CME, CML, SO,
674 KMW, and DAO conducted data analysis. TNG and KAW assisted with data analysis and
675 experimental design. CME and CML made the figures. TNG wrote the first draft of the manuscript.
676 CME, CML, and KAW assisted with writing and editing the manuscript. All authors approved the
677 manuscript. TNG, CME, and KAW acquired funding, and TNG and KAW supervised the project.
678
679 **DATA AVAILABILITY**
680 All data generated or analyzed during this study are included in the manuscript and supporting
681 file; Source Data files have been uploaded to Mendeley for all figures (doi:
682 10.17632/kt23th75v9.2). Code has been uploaded to GitHub
683 (https://github.com/doctheagrif/Current-Clamp-Matlab-Code_O-Neil-DA). A key resources table
684 with specific organism and reagent information has been included in the methods section.
685

686 **REFERENCES**
687
688 Ahern CA, Payandeh J, Bosmans F, Chanda B. 2016. The hitchhiker's guide to the voltage-gated
689 sodium channel galaxy. *J Gen Physiol* **147**:1–24. doi:10.1085/jgp.201511492

690 Alvarez FJ, Titus-Mitchell HE, Bullinger KL, Kraszpulski M, Nardelli P, Cope TC. 2011. Permanent
691 central synaptic disconnection of proprioceptors after nerve injury and regeneration. I. Loss of
692 VGLUT1/IA synapses on motoneurons. *J Neurophysiol* **106**:2450–2470.
693 doi:10.1152/jn.01095.2010

694 Aman TK, Grieco-Calub TM, Chen C, Rusconi R, Slat EA, Isom LL, Raman IM. 2009. Regulation
695 of persistent Na current by interactions between beta subunits of voltage-gated Na channels. *J*
696 *Neurosci* **29**:2027–2042. doi:10.1523/JNEUROSCI.4531-08.2009

697 Barbosa C, Tan Z-Y, Wang R, Xie W, Strong JA, Patel RR, Vasko MR, Zhang J-M, Cummins TR.
698 2015. Navβ4 regulates fast resurgent sodium currents and excitability in sensory neurons. *Mol*
699 *Pain* **11**:60. doi:10.1186/s12990-015-0063-9

700 Bean BP. 2007. The action potential in mammalian central neurons. *Nat Rev Neurosci* **8**:451–
701 465. doi:10.1038/nrn2148

702 Bennett DL, Clark AJ, Huang J, Waxman SG, Dib-Hajj SD. 2019. The Role of Voltage-Gated
703 Sodium Channels in Pain Signaling. *Physiol Rev* **99**:1079–1151.
704 doi:10.1152/physrev.00052.2017

705 Bewick GS, Banks RW. 2015. Mechanotransduction in the muscle spindle. *Pflugers Arch*
706 **467**:175–190. doi:10.1007/s00424-014-1536-9

707 Bewick GS, Reid B, Richardson C, Banks RW. 2005. Autogenic modulation of mechanoreceptor
708 excitability by glutamate release from synaptic-like vesicles: evidence from the rat muscle spindle
709 primary sensory ending. *J Physiol* **562**:381–394. doi:10.1113/jphysiol.2004.074799

710 Carrasco DI, Vincent JA, Cope TC. 2017. Distribution of TTX-sensitive voltage-gated sodium
711 channels in primary sensory endings of mammalian muscle spindles. *J Neurophysiol* **117**:1690–
712 1701. doi:10.1152/jn.00889.2016

713 Catterall WA. 2017. Forty Years of Sodium Channels: Structure, Function, Pharmacology, and
714 Epilepsy. *Neurochem Res* **42**:2495–2504. doi:10.1007/s11064-017-2314-9

715 Chang W, Berta T, Kim YH, Lee S, Lee S-Y, Ji R-R. 2018. Expression and Role of Voltage-Gated
716 Sodium Channels in Human Dorsal Root Ganglion Neurons with Special Focus on Nav1.7,
717 Species Differences, and Regulation by Paclitaxel. *Neurosci Bull* **34**:4–12. doi:10.1007/s12264-
718 017-0132-3

719 Claes L, Del-Favero J, Ceulemans B, Lagae L, Van Broeckhoven C, De Jonghe P. 2001. De novo
720 mutations in the sodium-channel gene SCN1A cause severe myoclonic epilepsy of infancy. *Am J*
721 *Hum Genet* **68**:1327–1332. doi:10.1086/320609

722 de Nooij JC, Doobar S, Jessell TM. 2013. Etv1 inactivation reveals proprioceptor subclasses that
723 reflect the level of NT3 expression in muscle targets. *Neuron* **77**:1055–1068.
724 doi:10.1016/j.neuron.2013.01.015

725 Ding J, Li X, Tian H, Wang L, Guo B, Wang Y, Li W, Wang F, Sun T. 2021. SCN1A Mutation-
726 Beyond Dravet Syndrome: A Systematic Review and Narrative Synthesis. *Front Neurol*
727 **12**:743726. doi:10.3389/fneur.2021.743726

728 Escayg A, Goldin AL. 2010. Sodium channel SCN1A and epilepsy: mutations and mechanisms.
729 *Epilepsia* **51**:1650–1658. doi:10.1111/j.1528-1167.2010.02640.x

730 Felts PA, Yokoyama S, Dib-Hajj S, Black JA, Waxman SG. 1997. Sodium channel alpha-subunit
731 mRNAs I, II, III, NaG, Na6 and hNE (PN1): different expression patterns in developing rat nervous
732 system. *Brain Res Mol Brain Res* **45**:71–82. doi:10.1016/s0169-328x(96)00241-0

733 Florez-Paz D, Bali KK, Kuner R, Gomis A. 2016. A critical role for Piezo2 channels in the
734 mechanotransduction of mouse proprioceptive neurons. *Sci Rep* **6**:25923.
735 doi:10.1038/srep25923

736 Fujiwara T, Sugawara T, Mazaki-Miyazaki E, Takahashi Y, Fukushima K, Watanabe M, Hara K,
737 Morikawa T, Yagi K, Yamakawa K, Inoue Y. 2003. Mutations of sodium channel alpha subunit
738 type 1 (SCN1A) in intractable childhood epilepsies with frequent generalized tonic-clonic seizures.
739 *Brain J Neurol* **126**:531–546. doi:10.1093/brain/awg053

740 Fukuoka T, Kobayashi K, Yamanaka H, Obata K, Dai Y, Noguchi K. 2008. Comparative study of
741 the distribution of the alpha-subunits of voltage-gated sodium channels in normal and axotomized
742 rat dorsal root ganglion neurons. *J Comp Neurol* **510**:188–206. doi:10.1002/cne.21786

743 Griffith TN, Docter TA, Lumpkin EA. 2019. Tetrodotoxin-Sensitive Sodium Channels Mediate
744 Action Potential Firing and Excitability in Menthol-Sensitive Vglut3-Lineage Sensory Neurons. *J*
745 *Neurosci* **39**:7086–7101. doi:10.1523/JNEUROSCI.2817-18.2019

746 He X-H, Zang Y, Chen X, Pang R-P, Xu J-T, Zhou X, Wei X-H, Li Y-Y, Xin W-J, Qin Z-H, Liu X-
747 G. 2010. TNF-α contributes to up-regulation of Nav1.3 and Nav1.8 in DRG neurons following
748 motor fiber injury. *Pain* **151**:266–279. doi:10.1016/j.pain.2010.06.005

749 Herzog RI, Cummins TR, Ghassemi F, Dib-Hajj SD, Waxman SG. 2003. Distinct repriming and
750 closed-state inactivation kinetics of Nav1.6 and Nav1.7 sodium channels in mouse spinal sensory
751 neurons. *J Physiol* **551**:741–750. doi:10.1113/jphysiol.2003.047357

752 Ho C, O'Leary ME. 2011. Single-cell analysis of sodium channel expression in dorsal root
753 ganglion neurons. *Mol Cell Neurosci* **46**:159–166. doi:10.1016/j.mcn.2010.08.017

754 Kalume F, Yu FH, Westenbroek RE, Scheuer T, Catterall WA. 2007. Reduced sodium current in
755 Purkinje neurons from Nav1.1 mutant mice: implications for ataxia in severe myoclonic epilepsy
756 in infancy. *J Neurosci* **27**:11065–11074. doi:10.1523/JNEUROSCI.2162-07.2007

Khaliq ZM, Gouwens NW, Raman IM. 2003. The contribution of resurgent sodium current to high-frequency firing in Purkinje neurons: an experimental and modeling study. *J Neurosci* **23**:4899–4912.

Kim AY, Tang Z, Liu Q, Patel KN, Maag D, Geng Y, Dong X. 2008. Pirt, a phosphoinositide-binding protein, functions as a regulatory subunit of TRPV1. *Cell* **133**:475–485. doi:10.1016/j.cell.2008.02.053

Kupari J, Usoskin D, Parisien M, Lou D, Hu Y, Fatt M, Lönnerberg P, Spångberg M, Eriksson B, Barkas N, Kharchenko PV, Loré K, Khoury S, Diatchenko L, Ernfors P. 2021. Single cell transcriptomics of primate sensory neurons identifies cell types associated with chronic pain. *Nat Commun* **12**:1510. doi:10.1038/s41467-021-21725-z

Lin S-H, Cheng Y-R, Banks RW, Min M-Y, Bewick GS, Chen C-C. 2016. Evidence for the involvement of ASIC3 in sensory mechanotransduction in proprioceptors. *Nat Commun* **7**:11460. doi:10.1038/ncomms11460

Lossin C. 2009. A catalog of SCN1A variants. *Brain Dev* **31**:114–130. doi:10.1016/j.braindev.2008.07.011

MacDonald DI, Sikandar S, Weiss J, Pyrski M, Luiz AP, Millet Q, Emery EC, Mancini F, Iannetti GD, Alles SRA, Arcangeletti M, Zhao J, Cox JJ, Brownstone RM, Zufall F, Wood JN. 2021. A central mechanism of analgesia in mice and humans lacking the sodium channel NaV1.7. *Neuron* **109**:1497-1512.e6. doi:10.1016/j.neuron.2021.03.012

Madisen L, Zwingman TA, Sunkin SM, Oh SW, Zariwala HA, Gu H, Ng LL, Palmiter RD, Hawrylycz MJ, Jones AR, Lein ES, Zeng H. 2010. A robust and high-throughput Cre reporting and characterization system for the whole mouse brain. *Nat Neurosci* **13**:133–140. doi:10.1038/nn.2467

780 Mulley JC, Scheffer IE, Petrou S, Dibbens LM, Berkovic SF, Harkin LA. 2005. SCN1A mutations
781 and epilepsy. *Hum Mutat* **25**:535–542. doi:10.1002/humu.20178

782 Nguyen MQ, von Buchholtz LJ, Reker AN, Ryba NJ, Davidson S. 2021. Single-nucleus
783 transcriptomic analysis of human dorsal root ganglion neurons. *eLife* **10**:e71752.
784 doi:10.7554/eLife.71752

785 Ogiwara I, Miyamoto H, Morita N, Atapour N, Mazaki E, Inoue I, Takeuchi T, Itohara S, Yanagawa
786 Y, Obata K, Furuichi T, Hensch TK, Yamakawa K. 2007. Nav1.1 localizes to axons of
787 parvalbumin-positive inhibitory interneurons: a circuit basis for epileptic seizures in mice carrying
788 an Scn1a gene mutation. *J Neurosci* **27**:5903–5914. doi:10.1523/JNEUROSCI.5270-06.2007

789 Oliver KM, Florez-Paz DM, Badea TC, Mentis GZ, Menon V, de Nooij JC. 2021. Molecular
790 correlates of muscle spindle and Golgi tendon organ afferents. *Nat Commun* **12**:1451.
791 doi:10.1038/s41467-021-21880-3

792 Osteen JD, Herzig V, Gilchrist J, Emrick JJ, Zhang C, Wang X, Castro J, Garcia-Caraballo S,
793 Grundy L, Rychkov GY, Weyer AD, Dekan Z, Undheim EAB, Alewood P, Stucky CL, Brierley SM,
794 Basbaum AI, Bosmans F, King GF, Julius D. 2016. Selective spider toxins reveal a role for the
795 Nav1.1 channel in mechanical pain. *Nature* **534**:494–499. doi:10.1038/nature17976

796 Patel RR, Barbosa C, Xiao Y, Cummins TR. 2015. Human Nav1.6 Channels Generate Larger
797 Resurgent Currents than Human Nav1.1 Channels, but the Navβ4 Peptide Does Not Protect
798 Either Isoform from Use-Dependent Reduction. *PloS One* **10**:e0133485.
799 doi:10.1371/journal.pone.0133485

800 Pineda-Farias JB, Loeza-Alcocer E, Nagarajan V, Gold MS, Sekula RF. 2021. Mechanisms
801 Underlying the Selective Therapeutic Efficacy of Carbamazepine for Attenuation of Trigeminal
802 Nerve Injury Pain. *J Neurosci* **41**:8991–9007. doi:10.1523/JNEUROSCI.0547-21.2021

Salvatierra J, Castro J, Erickson A, Li Q, Braz J, Gilchrist J, Grundy L, Rychkov GY, Deiteren A, Rais R, King GF, Slusher BS, Basbaum A, Pasricha PJ, Brierley SM, Bosmans F. 2018. NaV1.1 inhibition can reduce visceral hypersensitivity. *JCI Insight* **3**:121000. doi:10.1172/jci.insight.121000

Sharma N, Flaherty K, Lezgiyeva K, Wagner DE, Klein AM, Ginty DD. 2020. The emergence of transcriptional identity in somatosensory neurons. *Nature* **577**:392–398. doi:10.1038/s41586-019-1900-1

Than K, Kim E, Navarro C, Chu S, Klier N, Occiano A, Ortiz S, Salazar A, Valdespino SR, Villegas NK, Wilkinson KA. 2021. Vesicle-released glutamate is necessary to maintain muscle spindle afferent excitability but not dynamic sensitivity in adult mice. *J Physiol* **599**:2953–2967. doi:10.1113/JP281182

Usoskin D, Furlan A, Islam S, Abdo H, Lönnerberg P, Lou D, Hjerling-Leffler J, Haeggström J, Kharchenko O, Kharchenko PV, Linnarsson S, Ernfors P. 2015. Unbiased classification of sensory neuron types by large-scale single-cell RNA sequencing. *Nat Neurosci* **18**:145–153. doi:10.1038/nn.3881

Wang W, Atianjoh F, Gauda EB, Yaster M, Li Y, Tao Y-X. 2011. Increased expression of sodium channel subunit Nav1.1 in the injured dorsal root ganglion after peripheral nerve injury. *Anat Rec Hoboken NJ 2007* **294**:1406–1411. doi:10.1002/ar.21437

Waxman SG, Kocsis JD, Black JA. 1994. Type III sodium channel mRNA is expressed in embryonic but not adult spinal sensory neurons, and is reexpressed following axotomy. *J Neurophysiol* **72**:466–470. doi:10.1152/jn.1994.72.1.466

Wilkinson KA, Kloefkorn HE, Hochman S. 2012. Characterization of muscle spindle afferents in the adult mouse using an in vitro muscle-nerve preparation. *PloS One* **7**:e39140. doi:10.1371/journal.pone.0039140

827 Woo S-H, Lukacs V, de Nooij JC, Zaytseva D, Criddle CR, Francisco A, Jessell TM, Wilkinson
828 KA, Patapoutian A. 2015. Piezo2 is the principal mechanotransduction channel for proprioception.
829 *Nat Neurosci* **18**:1756–1762. doi:10.1038/nn.4162

830 Wu H, Petitpré C, Fontanet P, Sharma A, Bellardita C, Quadros RM, Jannig PR, Wang Y, Heimel
831 JA, Cheung KKY, Wanderoy S, Xuan Y, Meletis K, Ruas J, Gurumurthy CB, Kiehn O, Hadjab S,
832 Lallemend F. 2021. Distinct subtypes of proprioceptive dorsal root ganglion neurons regulate
833 adaptive proprioception in mice. *Nat Commun* **12**:1026. doi:10.1038/s41467-021-21173-9

834 Yu FH, Mantegazza M, Westenbroek RE, Robbins CA, Kalume F, Burton KA, Spain WJ, McKnight
835 GS, Scheuer T, Catterall WA. 2006. Reduced sodium current in GABAergic interneurons in a
836 mouse model of severe myoclonic epilepsy in infancy. *Nat Neurosci* **9**:1142–1149.
837 doi:10.1038/nn1754

838 Zheng Y, Liu P, Bai L, Trimmer JS, Bean BP, Ginty DD. 2019. Deep Sequencing of
839 Somatosensory Neurons Reveals Molecular Determinants of Intrinsic Physiological Properties.
840 *Neuron* **103**:598-616.e7. doi:10.1016/j.neuron.2019.05.039

841